Wind-wave interaction in finite depth: linear and nonlinear approaches, blow-up and soliton breaking in finite time, integrability perspectives

A. Latifi

Department of Mechanics, Faculty of Physics,
Qom University of Technology
Qom, Iran

M.A. Manna

Université de Montpellier (UM)
and
Conseil National de la Recherche Scientifique (CNRS),
Laboratoire Charles Coulomb UMR 5221
F-34095, Montpellier, France

R.A. Kraenkel

Instituto de Física Téorica, UNESP
Universidade Estadual Paulista
01140-070, São Paulo, Brazil

Abstract

This work is a review of our recent analytical advances of the evolution of surface water solitary waves in Miles and Jeffreys' theories of wind wave interaction in water of finite depth. Although many works have been conducted based on Miles and Jeffreys' approach, only a few studies have been carried out on finite depth. The present review is divided into two major parts. The first corresponds to the surface water waves in a linear regime and its nonlinear extensions. In this part, Miles' theory of wave amplification by wind is extended to the case of finite depth. The dispersion relation provides a wave growth rate depending on depth. A dimensionless water depth parameter, depending on the depth and a characteristic wind speed, induces a

family of curves representing the wave growth as a function of the wave phase velocity and the wind speed. Our theoretical results are in good agreement with the data from the Australian Shallow Water Experiment and the data from the Lake George experiment. In the second part of this study, Jeffreys' theory of wave amplification by wind is extended to the case of finite depth, where the fully nonlinear focusing Serre-Green-Naghdi (SGN) equation is derived. "Anti-dissipation" occurs due to the continuous transfer of wind energy to water surface waves. We find the solitary wave solution of the system, with an increasing amplitude under the action of the wind. This continuous increase in amplitude leads to the "soliton" breaking and blow-up of the surface wave in finite time for infinitely large asymptotic space. This dispersive, focusing and fully nonlinear phenomenon is equivalent to the linear instability at infinite time. The theoretical blow-up time is calculated based on actual experimental data. By applying an appropriate perturbation method, the SGN equation yields a focusing weakly nonlinear dispersive Korteweg–de Vries–Burger-type (KdV-B) equation. We show that the continuous transfer of energy from wind to water results in the growth of the KdV-B soliton-like's amplitude, velocity, acceleration, and energy over time while its effective wavelength decreases. This phenomenon differs from the classical results of Jeffreys' approach due to finite depth. Again, blow-up and breaking occur in finite time. These times are calculated and expressed for solitary wave solution- and wind-appropriate parameters and values. These values are measurable in usual experimental facilities. The kinematics of the breaking is studied, and a detailed analysis of the breaking kinetics and breaking time is conducted using various criteria. Finally, some integrability perspectives are presented.

1   Introduction

The Navier-Stokes equation for air and water is the starting point of wind-generated water waves. Since the Navier-Stokes equation is analytically unsolved, various approximations and assumptions are required to obtain particular solutions.

The wind wave growth is due to the continuous energy and momentum flow from the air to the water. Winds generate surface waves; in turn, surface water waves modify the airflow. In this way, the atmosphere depends on the wave state near the water surface. The physical mechanism behind is "focusing" with a continuous energy and momentum flow from the air to the surface wave generating an exponential growth of the wave amplitude in time, more or less quickly, depending on the wind speed and the water depth.

However, waves may lose energy because of dissipation. The *action balance equation*, a fundamental equation in fluid dynamics, commonly represents this temporal and spatial dynamics. In deep water, it reads [1]:

$$\frac{\partial}{\partial t}\mathcal{N} + \overrightarrow{\nabla}.(\overrightarrow{c_g}\mathcal{N}) = S, \tag{1}$$

where $\overrightarrow{c_g}$ is the group velocity observed in a frame moving with the wave, $\mathcal{N}$ is *the action density* defined as follows:

$$\mathcal{N} = \frac{\mathcal{E}}{\omega}, \tag{2}$$

where ω is the wave frequency, $\mathcal{E}$ is the energy density

$$\mathcal{E} = 2\rho_w g \eta_0^2, \tag{3}$$

where η_0 the small wave amplitude, and S is the source term

$$S = S_{in} + S_{nl} + S_{ds} + \dots, \tag{4}$$

where S_{in}, S_{nl}, S_{ds} are the effects of the wind input, non-linear interactions and dissipation due to white capping, respectively.

The pioneer theoretical works on surface wind-wave growth were essentially done by Jeffreys and Miles [2–5], till some more recent studies [6, 7]. These works essentially aim to compute the term S_{in} in Eq. (4). Later, numerical approaches attempted to campute S_{in}, S_{nl}, S_{ds} [1].

However, all theories mentioned above are focused on *deep water domain* and are not well adapted to correctly describe wind-waves generation near-shore oceans or shallow lakes. This limitation challenges both the physics and engineering communities. Indeed, in the *finite depth water domain* the source term is

$$S = S_{in} + S_{nl} + S_{ds} + S_{bf} + S_{tri} + \dots. \tag{5}$$

where S_{bf} is the bottom friction, and S_{tri} is triad nonlinear wave interactions. Moreover, S_{in} being strongly influenced by the finite depth h, must be recalculated. To our knowledge, although many works have been conducted based on Miles and Jeffreys' approach, only a few studies are carried out on finite depth [8–11].

This review is the result of our analytical extension of the evolution of surface water solitary waves in Miles and Jeffreys' theories of wind wave interaction in water of finite depth with the Euler equations as outset. The analytic approach is essential for further numerical investigations due to the scale of energy dissipation near coasts. Indeed, the scale of energy dissipation is of the order of a micrometre, which requires 10^{25} mesh nodes to produce correct predictions on scales of 100 km. Hence, no pure numerical modelling of this problem without recourse to theoretical developments has a chance of succeeding.

Based on the our latest progress [8–11], this work aims to give *l'etat de l'art* in the field of wind-wave interactions in finite depth, and thereby supply a theoretical basis allowing to go beyond the empirical laws. A permanent concern in this work is to compare our theoretical results to experimental data or check the feasibility of experimentation and field observations.

This paper is divided into two parts: The first part is dedicated to the extension of Miles' approach [5] to finite depth, where the linearized Euler equations in the water domain are coupled with weak nonlinearity to linearized Euler equations in the air domain. The problem is solved at the interface, and the linear dispersion relation of wave amplification at finite depth is calculated. By introducing dimensionless variables and scaling, the wind wave's growth rate is obtained. Our theoretical laws are compared with both the Young-Verhagen data and plots of empirical relationships from the Lake George experiment and with Donelan's data from the AUSWEX program [12–14].

Introducing a simple *modus operandi* for the Miles' mechanism allows us to derive an anti-diffusive nonlinear Schrödinger equation for the wind-wave in finite depth and we derive the Akhmediev, Peregrine, and Ma solutions for weak wind inputs.

The second part of this paper is devoted to the extension of Jeffrey's mechanism [2,3] where in different scales, the focusing KdV-B equation and the fully nonlinear SGN are derived. The focusing KdV-B equation is obtained by the coupling of the weakly nonlinear Euler equations in the water domain to the linearized Euler equations in the air domain. In contrast, the fully nonlinear SGN is derived by coupling the nonlinear Euler equations in the water domain to the linearized Euler equations in the air domain.

For both SGN and KdV-B equations, solitary waves solutions exhibiting blow-up in finite time are found. By considering its kinematics description, the solition breaking phenomenon is analyzed in detail in the case of KdV-B equation.

This review is organized as follows: Section 2 studies the mutual action of linearised water and air dynamics through Mile's mechanism in finite depth. The wave growth rate is analytically calculated and compared to field experiment results and empiric laws. A good agreement between theoretical and experimental results is observed. Section 3 compares our theoretical results to experimental and empirical laws. In Section 3, we apply the Miles approach from a quasi-linear perspective. Here, the air dynamics remain linear, while the water domain is viewed as irrotational and nonlinear. This modification gives rise to the Nonlinear Schrödinger equation, from which we derive the Akhmedeiev, Peregrine, and Ma solutions solutions for weak wind input. Sections 4 and 5 are devoted to the nonlinear Jeffrey's approach. Namely, in section 3, the water domain is considered irrotational and nonlinear, and the air domain is linearized. Jeffrey's sheltering mechanism allows us to derive the SGN equation in finite depth, which we solve analytically. The solution is a solitary wave with the remarkable feature of blowing up in finite time. The blow-up time is calculated based on experimental measurement. In section 5, applying an appropriate approximation, we derive the KdV-B equation from the SGN equation we solve analytically. Again, the solution is a solitary wave with a blow-up in finite time. In this section, we conduct a detailed analysis of the wave breaking before the blow-up, which we compare to existing breaking criteria. In Section 6, we present some integrability perspectives. Section 7 summarises our results, draws conclusions, and gives perspectives on further developments. In the Appendix, the direct derivation of the KdV-B equation Euler equation is shown.

2   Mile's Mechanism

The Miles mechanism in infinite or finite depth is based on a particular interaction between air flows and surface waves. It's about a linear mechanism of resonance between the wind speed and the water phase speed, which will induce a change in pressure and modify the propagation properties of linear water surface waves. We therefore model this instability as follows: either a coordinate system Cartesian dimensions with x the horizontal, z the height and y the transverse dimension, which we will not consider here. We consider two fluids, air and water, separated by a free surface (x, t). The constant densities of air and water are ρ_a and ρ_w. Pressure fields in water and air are denoted respectively P_w and P_a. The bottom is located at a depth $z = -h$ and the interface $z = \eta(x, t)$. We prescribe a wind $U(z)$ having a specific profile, typically logarithmic, as in Figure (1). Therefore, we will write Euler's equations for air and water, with an additional condition of pressure continuity connecting them. We assume the dynamic to be linear and disregard the air
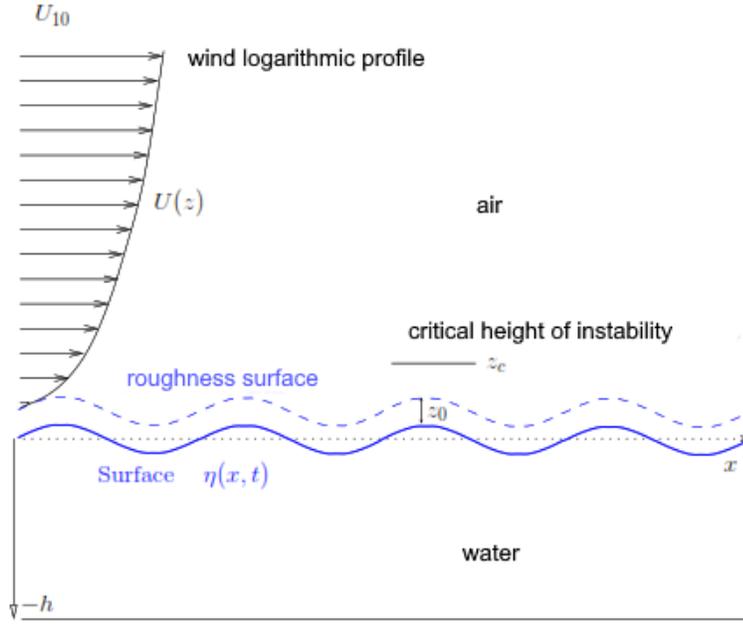
Figure 1. The Miles mechanism is based on a particular interaction between air flows and surface waves. It's about a linear mechanism of resonance between the wind speed and the water phase speed, which will induce a change in pressure, which in turn will modify the propagation properties of linear water surface waves. We consider two fluids, air and water, separated by a free surface (x, t). The bottom is located at a depth $-h$, and we prescribe a wind $U(z)$ having a specific profile, typically logarithmic. The interface at rest. The perturbed air-water interface will be described by $z = \eta(x, t)$.

turbulence, building a *quasi-laminar theory*.

2.1   The linearized water dynamics

In the water domain, we consider the Euler equations for finite depth. The horizontal and vertical velocities of the fluid are $u(x, z, t)$ and $w(x, z, t)$. The continuity equation and the linearized equation of motion in the water domain read [15]:

$$u_x + w_z = 0, \quad \rho_w u_t = -P_x, \quad \rho_w w_t = -P_z - g\rho_w, \tag{6}$$

where $P(x, z, t)$ is the pressure, g the gravitational acceleration, ρ_w is the water density and subscripts in u, w, P_x and P_z denote partial derivatives of P with respect to x and z, receptively. The boundary conditions at $z = -h$ and at $z = \eta(x, t)$ are

$$w(-h) = 0, \quad \eta_t = w(0), \tag{7}$$
$$P(x, \eta, t) = P_a(x, \eta, t), \tag{8}$$

where P_a is the air pressure evaluated at $z = \eta$. Thus equation (8) is the continuity of the pressure across the air/water interface. As this is a vital assumption for the growth

mechanism, we give it a more pleasant expression. So, let us introduce a reduced pressure defined by

$$\mathbf{P}(x, z, t) = P(x, z, t) + \rho_w g z - P_0, \tag{9}$$

where P_0 is the atmospheric pressure. In terms of (9) equations (6)-(8) read

$$u_x + w_z = 0, \quad \rho_w u_t = -\mathbf{P}_x, \quad \rho_w w_t = -\mathbf{P}_z, \tag{10}$$

$$w(-h) = 0, \quad \eta_t = w(0), \tag{11}$$

$$\mathbf{P}(x, \eta, t) = P_a(x, \eta, t) + \rho_w g \eta - P_0. \tag{12}$$

The linear equations system (10)-(12) can be solved, assuming normal mode solutions as

$$\begin{aligned} \mathbf{P} &= \mathcal{P}(z) \exp(i\theta), \quad u = \mathcal{U}(z) \exp(i\theta), \\ w &= \mathcal{W}(z) \exp(i\theta), \quad \eta = \eta_0 \exp(i\theta), \end{aligned} \tag{13}$$

with $\theta = k(x - ct)$ where k is the wavenumber, c the phase speed and η_0 is a constant. Using equations (10), (11), (12) and (13) we obtain

$$w(x, z, t) = \frac{-ikc \sinh k(z + h)}{\sinh kh} \eta_0 \exp(i\theta), \tag{14}$$

$$u(x, z, t) = \frac{kc \cosh k(z + h)}{\sinh kh} \eta_0 \exp(i\theta), \tag{15}$$

$$\mathbf{P}(x, z, t) = \frac{k \rho_w c^2 \cosh k(z + h)}{\sinh kh} \eta_0 \exp(i\theta). \tag{16}$$

The phase speed c is unknown in equations (14)-(16). To determine c we have to consider the boundary conditions (12), not yet used, and (11) which yields

$$\rho_w \eta_0 \exp(i\theta)\{c^2 k \coth kh - g\} + P_0 = P_a(x, \eta, t). \tag{17}$$

In the single-domain problem $P_a(x, \eta, t) = P_0$ and (17) gives the usual expression for c,

$$c^2 = c_0^2 = \frac{g}{k} \tanh(kh). \tag{18}$$

It is not the case in the problem under consideration in the present paper in which the determination of c needs the use of the air pressure evaluated at $z = \eta$.

2.2   The linearized air dynamics

Let us consider the linearized governing equation of a steady airflow, with a prescribed mean horizontal velocity $U(z)$ depending on the vertical coordinate z. We are going to study perturbations to the mean flow $U(z)$: $u_a(x, z, t)$, $w_a(x, z, t)$ and $P_a(x, z, t)$ where subscript a stands for air. So with $\mathbf{P}_a(x, z, t) = P_a(x, z, t) + \rho_a g z - P_0$, ρ_a the air density, and $U' = dU(z)/dz$ we have the following equations

$$u_{a,x} + w_{a,z} = 0, \tag{19}$$

$$\rho_a[u_{a,t} + U(z)u_{a,x} + U'(z)w_a] = -\mathbf{P}_{a,x}, \tag{20}$$

$$\rho_a[w_{a,t} + U(z)w_{a,x}] = -\mathbf{P}_{a,z}, \tag{21}$$

which must be completed with the appropriate boundary conditions. The first is the kinematic boundary condition for air, evaluated at the aerodynamic sea surface roughness z_0 located just above the interface. Through this paper, z_0 will be regarded as a constant independent from the sea state. This is a widely used approximation, first proposed by [16]. For the datasets used later on, the wind speed ranges are such that the roughness may be seen as a constant [17]. The kinematic boundary condition reads

$$\eta_t + U(z_0)\eta_x = w_a(z_0). \tag{22}$$

We choose $U(z)$ as the logarithmic wind profile. This is commonly used to describe the vertical distribution of the horizontal mean wind speed within the lowest portion of the air side of the marine boundary layer [18]. It can also be justified with scaling arguments and solution matching between the near-surface and geostrophic air layer [19].

$$U(z) = U_1 \ln(z/z_0), \quad U_1 = \frac{u_*}{\kappa}, \quad \kappa \approx 0.41, \tag{23}$$

where u_* is the friction velocity and κ the Von Kármán constant. So, eq. (22) can be reduced to

$$\eta_t = w_a(z_0). \tag{24}$$

This equation describes the influence of the surface perturbation on the vertical perturbed wind speed. Next we assume $\mathbf{P}_a = \mathcal{P}_a(z)\exp(i\theta)$, $u_a = \mathcal{U}_a(z)\exp(i\theta)$, $w_a = \mathcal{W}_a(z)\exp(i\theta)$ and we add the following boundary conditions on $\mathcal{W}_a$ and $\mathcal{P}_a$,

$$\lim_{z \to +\infty} (\mathcal{W}'_a + k\mathcal{W}_a) = 0, \tag{25}$$

$$\lim_{z \to z_0} \mathcal{W}_a = W_0, \tag{26}$$

$$\lim_{z \to +\infty} \mathcal{P}_a = 0, \tag{27}$$

that is, the disturbance plus its derivative vanish at infinity, and the vertical component of the wind speed is enforced by the wave movement at the sea surface. Then, using equations (19)-(21) and (27) we obtain

$$w_a(x, z, t) = \mathcal{W}_a \exp(i\theta), \tag{28}$$

$$u_a(x, z, t) = \frac{i}{k}\mathcal{W}_{a,z}\exp(i\theta), \tag{29}$$

$$\mathbf{P}_a(x, z, t) = ik\rho_a \exp(i\theta) \int_z^\infty [U - c]\mathcal{W}_a dz'. \tag{30}$$

Removing the pressure from the Euler equations, we find the well-known Rayleigh equation [20] $\forall z \setminus z_0 < z < +\infty$ (inviscid Orr-Sommerfeld equation)

$$(U - c)(\mathcal{W}''_a - k^2\mathcal{W}_a) - U''\mathcal{W}_a = 0 \tag{31}$$

which is singular at the critical, or matched height $z_c = z_0 e^{c\kappa/u_*} > z_0 > 0$, where $U(z_c) = c$. We recall that this model disregards any kind of turbulence, and so the critical height is set above any turbulent eddies or other non-linear phenomena. In equations (28)-(31)

neither $\mathcal{W}_a(z)$ nor c are known. In order to find c, we have to calculate $P_a(x, \eta, t)$. We obtain

$$P_a(x, \eta, t) = P_0 - \rho_a g \eta + ik\rho_a \exp{(i\theta)} \int_{z_0}^{\infty} [U(z) - c]\mathcal{W}_a(z)dz, \tag{32}$$

where the lower integration bound is taken at the constant roughness height z_0 instead of $z = \eta$ since we are studying the linear problem. Using equation (24) to eliminate the term $ik\rho_a \exp(i\theta)$ the equation (32) in (17) yields

$$g(1 - s) + c\frac{sk^2}{W_0}I_1 - c^2\{\frac{sk^2}{W_0}I_2 + k\coth(kh)\} = 0, \tag{33}$$

where $s = \rho_a/\rho_w$ and the integrals I_1 and I_2 are defined as follow

$$I_1 = \int_{z_0}^{\infty} U\mathcal{W}_a dz, \quad I_2 = \int_{z_0}^{\infty} \mathcal{W}_a dz. \tag{34}$$

Equation (33) is the dispersion relation of the problem. The parameter s is small ($\rho_a/\rho_w \sim 10^{-3}$) and (33) may be approximated as

$$c = c_0 + sc_1 + O(s^2). \tag{35}$$

The explicit form of c_1 is calculated in the next section. Therefore, we can find $\mathcal{W}_a(z)$ by solving (31) with c replaced by c_0, that is to say, of order zero in s.

2.3   The wave growth rate

The function $\mathcal{W}_a(z)$ is complex and consequently c also. Its imaginary part gives the growth rate of $\eta(x, t)$ defined by

$$\gamma = k\Im(c), \tag{36}$$

where $\Im(c)$ is the imaginary part of c. The theoretical and numerical results concerning the growth rate γ are studied and computed with two dimensionless parameters δ (see [12] and [13]) and θ_{dw} defined by

$$\delta = \frac{gh}{U_1^2}, \quad \theta_{dw} = \frac{1}{U_1}\sqrt{\frac{g}{k}}. \tag{37}$$

The dimensionless parameter δ, for constant U_1, measures the influence of the finite fluid depth on the rate of growth of $\eta(x, t)$. The parameter θ_{dw} can be seen as a *theoretical analogous of the deep water wave age*. It measures the relative value of the deep water phase speed about the characteristic wind velocity U_1. Now a *theoretical analogous of the finite depth wave age* θ_{fd} can be introduced as

$$\theta_{fd} = \frac{1}{U_1}\sqrt{\frac{g}{k}}\sqrt{\tanh(kh)} = \theta_{dw}T^{1/2}, \tag{38}$$

where

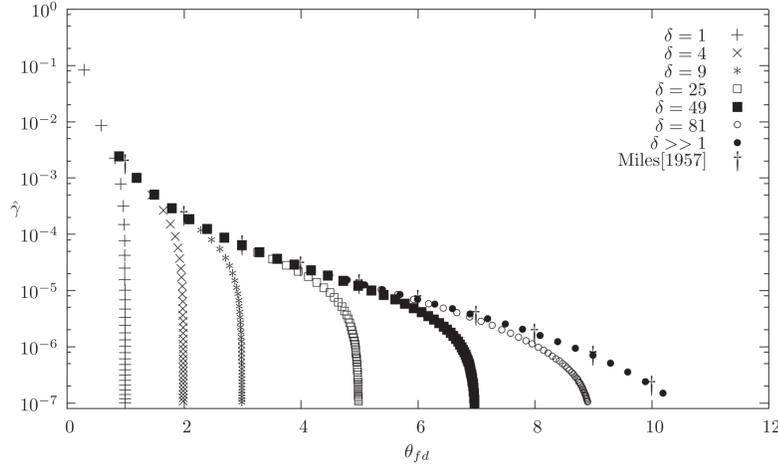$$T = \tanh(\frac{\delta}{\theta_{dw}^2}). \tag{39}$$

Figure 2. Evolution of the growth rate in semi-logarithmic scale. Every curve but the rightmost one correspond to finite depth. From left to right, they match $\delta = 1, 4, 9, 25, 49, 81$. We can observe that for each depth, there is a θ_{fd} – limited wave growth. The deep water limit, also computed, is corresponds to small θ_{fd} and matches Miles' results.

The form (38) is a depth weighted parameter such that for a finite and constant θ_{dw} we have $\theta_{fd} \sim \theta_{dw}$ if $\delta \to \infty$ and $\theta_{fd} \sim \delta^{1/2} = \sqrt{gh}/U_1$ if $\delta \to 0$. To obtain the growth rate, we introduce the following non-dimensional variables and scalings, hats meaning dimensionless quantities

$$U = U_1\hat{U}, \quad \mathcal{W}_a = W_0\hat{\mathcal{W}}_a, \quad z = \frac{\hat{z}}{k},$$

$$c = U_1\hat{c}, \quad t = \frac{U_1}{g}\hat{t}. \tag{40}$$

Using (37) and (40) in equation (33) and retaining only the terms of order one in s we obtain c,

$$\hat{c} = \hat{c}(\delta, \theta_{dw}) = \theta_{dw}T^{1/2} - \frac{s}{2}\theta_{dw}T^{1/2} + \frac{s}{2}\{T\hat{I}_1 - \theta_{dw}T^{3/2}\hat{I}_2\}, \tag{41}$$

and with $e^{\gamma t} = e^{k\Im(c)t} = e^{\Im(\hat{c})\hat{t}/\theta_{dw}^2}$, we have the dimensionless growth rate $\hat{\gamma} = \frac{U_1}{g}\gamma$ as,

$$\hat{\gamma} = \frac{s}{2}\{\frac{T\Im(I_1)}{\theta_{dw}^2} - \frac{T^{3/2}\Im(I_2)}{\theta_{dw}}\}, \tag{42}$$

So, we can compute it for a given (δ, θ_{dw}) set. The δ parameter does not appear explicitly, allowing us to compute γ for an infinite depth, where we have just $T \to 1$. This gives back to Miles' theory.

The existence of a finite depth h transforms the unique curve of wave growth rate in deep water in a *family of curves* indexed by $\delta = gh/U_1^2$, i.e., a curve for each value of δ. In Figure 2 shows a family of six values of δ against the θ_{fd} parameter. The limit $\delta \to \infty$ is included as well. Small finite θ_{fd} corresponds to short surface waves. This stage represents the initial growth of the wave field near the shoreline of a calm lake. As
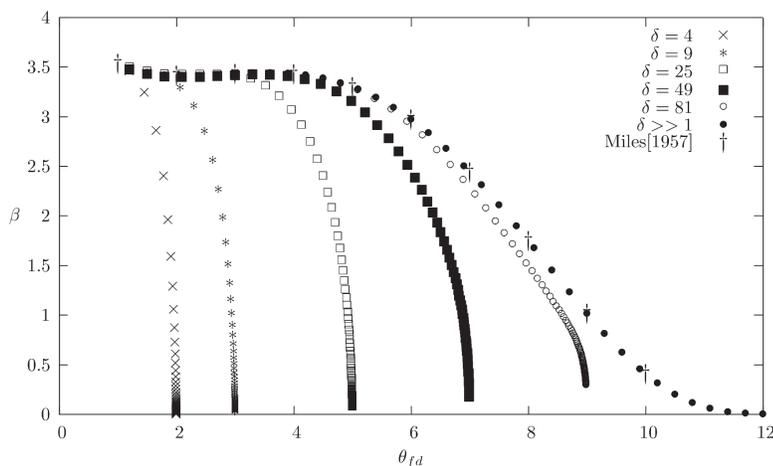
Figure 3. Evolution of Miles' coefficient β for several values of the depth. Each curve is plotted with the same Charnock constant $\alpha_c \approx 0.018$. The finite-depth effect is critical, and high value of δ correspond to deep water.

time proceeds, the surface waves reach moderate θ_{fd}, corresponding to mild or moderate wavelengths, while long waves are found for large θ_{fd}. Of course, as the wavelengths increase, the amplitudes keep on growing. Clearly, from a physical point of view, this means that Figure 2 is a snapshot of the theoretical dynamical development of the wave, which is growing in amplitude and wavelength in time.

Figure 2 shows that at small θ_{fd} the growth rate γ is equal for all values of δ, the limit being the deep water case. The finite-depth effects appear as θ_{fd} increases. The growth rate becomes lower than in the deep water limit for each value of δ. The growth rates are scaled with δ: for a given θ_{fd}, the bigger the δ the larger the $\hat{\gamma}$. Each δ-curve approaches its own (idealized) *theoretical θ_{fd}-limited growth* as $\hat{\gamma}$ goes to zero. At this stage, the wave reaches a final linear progressive wave with zero growth. In other words, for a given δ the surface wave does not grow old beyond a determined θ_{fd}.

In contrast to the usual analysis of wind-wave growth, our results concern the dimensionless growth rate $\hat{\gamma}$ instead of the β-Miles parameter. We have the following transformation rule between this parameter β and dimensionless $\hat{\gamma}$

$$\beta = \frac{2\hat{\gamma}}{s}\theta_{dw}^3 T^{1/2}, \tag{43}$$

where we took β as it is usually defined, with the dimensions, $\Im(c) = c_0\frac{s}{2}\beta(\frac{U_1}{c_0})^2$. This definition of Miles' β in finite depth is straightforward. Its evolution is shown clearly in Figure 3, showing the correct deep water trends and the new finite depth limits. The effects of depth are critical. As usual, β is almost constant for small θ_{fd}, but it goes dramatically to zero when the depth limit is close.

2.4   Field experiments on growth of surface wind-waves

For finite depth wave growth the pioneer experiments and numerical studies were conducted by [14,21,22] and particularly the experiments in Lake George, Australia, described

by [12]. They provided one of the first systematic attempts to understand the physics of wave-wind generation in finite-depth water.

The results of the field experiments in fetch limited growth have been presented in references [12] and [13]. These papers described the basin geometry and bathymetry, experimental design, used instrumentation, and the adopted scaling parameters. The measurements have confirmed the water depth dependence of the asymptotic limits to wave growth.

In reference [23] (see also [24]) derived an empirical relation in terms of appropriate dimensionless parameters able to reproduce the experimental data of [12]. In particular, the empirical relationship between the fractional energy increase as a function of the inverse wave age, found by [25] For deep water, it was extended to the finite depth domain. Experimental results and plots of the empirical laws have shown that contrary to the deep water case, the wave age at which the growth rate becomes zero is wind-dependent and depth-dependent. So, the point of full development is warped from the deep water case, where established it [26]. As a result, a growth law against the inverse wave age exists for each value of a parameter, which unites the dependences on wind intensity and water depth.

The evolution of the growth rates is such that at small wave ages, growth rates are comparable to the deep water limit at large wave ages, the growth rate is lower the growth rate vanishes beyond a limit wave age in shallow water than in deep water.

2.5 Comparisons with field experiments

In this subsection, we are going to show that our analytical and numerical results can reproduce qualitatively these experimental facts. At this point, it is essential to keep in mind that we are studying the linear growth of a normal Fourier mode k and not the growth of a wave train as the infinite superposition of wave Fourier modes.

Moreover, results in field or laboratory experiments are commonly given using the parameter C_p, the observed phase speed at the peak frequency ω_p. Consequently, qualitative comparison with field observations can only be made using the phase velocity c or frequency ω of one mode instead of C_p or ω_p.

We are going to show that the theoretical curves for $\hat{\gamma}$ are, *mutatis mutandi*, in good qualitative agreement with the empirical curves of the dimensionless fractional wave energy increase per radian $\hat{\Gamma}$ as a function of the inverse wave age U_{10}/Cp in [23]. In this reference, experimental field data for $\hat{\Gamma}$ in the finite depth of the empirical relationship adequately represents Lake George

$$
\begin{aligned}
\hat{\Gamma} &= \frac{C_g}{\omega_p} \frac{1}{E} \frac{\partial E}{\partial x} \\
&= A \left(\frac{U_{10}}{C_p} - 0,83 \right) \tanh^{0,45} \left(\frac{U_{10}}{C_p} - \frac{1,25}{\delta_Y^{0,45}} \right),
\end{aligned}
\tag{44}
$$

with A constant, $\delta_Y = gh/U_{10}^2$ the non-dimensional water depth, U_{10} the wind velocity at $10\ m$, and C_g and C_p the group and phase speeds of the components at the spectral peak frequency ω_p.

In order to make a qualitative comparison between $\hat{\Gamma}$ curves in function of the inverse wave-age U_{10}/C_p and theoretical $\hat{\gamma}$ curves in function of $1/\theta_{fd}$ we need to write the

empirical $\hat{\Gamma}$ in terms of theoretical quantities. So, the following changes are necessary:

$$\text{measured} \quad C_g, C_p, \omega_p \rightarrow \text{theoretical} \quad c_g, c, \omega, \tag{45}$$

$$\text{and} \qquad \frac{U_{10}C_{10}^{1/2}}{\kappa} = u_*/\kappa = U_1 \tag{46}$$

with C_{10} the 10 m drag coefficient [27]. Thus, from the fact that the energy growth rate is two times the amplitude growth rate, that is

$$\Gamma = 2\gamma,$$

and using $2c_g = c(1 + 2kh/\sinh(2kh))$, (45), (46),(38) and (40) we obtain

$$\hat{\Gamma} = \frac{\theta_{dw}}{T^{1/2}}\hat{\gamma}[1 + \frac{2\delta}{\theta_{dw}^2 \sinh(\frac{2\delta}{\theta_{dw}^2})}]. \tag{47}$$

This expression gives the theoretical equivalent of the empirical $\hat{\Gamma}$ in function of θ_{dw}, δ and $\hat{\gamma}$. The values of $\hat{\gamma}$ for fixed δ's as a function of $1/\theta_{fd}$ are numerically obtained from Eqs. (38) (39) and (42). Steps (45) and (46) transform δ_Y and C_p/U_{10} into δ and θ_{fd} according to

$$\delta_Y = \delta\frac{C_{10}}{\kappa^2}, \tag{48}$$

$$\frac{C_p}{U_{10}} = \theta_{fd}\frac{C_{10}^2}{\kappa}. \tag{49}$$

In reference [23] the curves of Γ versus U_{10}/C_p have been presented for the δ_Y-intervals $\delta_Y \in [0.1 - 0.2], [0.2 - 0.3], [0.3 - 0.4], [0.4 - 0.5]$, rather than for a single value of δ_Y. The intervals were determined from the variations in U_{10}, the depth h being nearly constant around 2 m. Consequently we substitute the δ_Y-intervals with δ-intervals using (48) and we evaluate the mean value $\bar{\delta}$. For example $\delta_Y \in [0, 1 - 0, 2]$ is transformed into $\delta = [13, 17 - 26, 35]$ with $\bar{\delta} = 19, 76$ in Figure 4(a). Figures 4(a), 4(b), 4(c) and 4(d) are displaying a fair concordance of the model with the experimental data and plots of empirical laws for Lake George. The agreement improves as $\frac{1}{\theta_{fd}}$ increases.

In Figure 5 are plotted, against δ, the critical values of the parameter θ_{fd}^c for which the growth rate γ goes to zero. They obey the relation

$$\theta_{fd}^c = \delta^{0,5}. \tag{50}$$

The above relation, found numerically, is coherent with the parameter formulation (38). It is indeed a limiting value for θ_{fd} uniquely determined by the water depth. In [23] the author has shown from an empirical relationship (formula (6) in reference above) that $\hat{\Gamma}$ the growth rate goes to zero as a function of the inverse wave age U_{10}/C_p for

$$\frac{C_p}{U_{10}} = 0.8(\frac{gh}{U_{10}^2})^{0.45}. \tag{51}$$

Using a C_{10} drag coefficient parametrization such as [27]

$$C_{10} = (0.065U_{10} + 0.8)10^{-3}, \tag{52}$$

and taking an average $U_{10} = 7\ m/s$ in [23], one finds the U_1 to U_{10} relationship

$$U_{10} \approx 28,3\ u_* \approx 11,6\ U_1, \tag{53}$$

So, this limiting law reads

$$\frac{C_p}{U_1} = 1,01\ \delta^{0,45}. \tag{54}$$

a result in excellent agreement with the theoretical value (50). With θ_{fd}^c we can calculate the corresponding critical wave length λ^c. Using (50) in (38) we obtain

$$\frac{\delta}{\theta_{dw}^2} = \tanh\left(\frac{\delta}{\theta_{dw}^2}\right). \tag{55}$$

Relation (55) means the wave has entered the shallow water region. In such a limit the range of δ/θ_{dw}^2 is: $0 < \delta/\theta_{dw}^2 < \frac{\pi}{4}$ ([28,29]). As a result we obtain $\lambda^c = 8h$. For values of λ such that $\lambda > \lambda^c$ the phase velocity is in the long wave limit i.e., $c = \sqrt{gh}$. Consequently, if $\lambda > \lambda_c$ the wave feels the bottom, the amplitude does not grow anymore, the resonance wind/phase speed ceases, and the wave reaches its utmost state as a progressive plane wave.

Finally in Figure 5 are also represented data from [25], from the Australian Shallow Water Experiment. A fit is also plotted to show the trend. The raw data consists in the water depth h in meters, the friction velocity u_*, the 10 meters wind velocity U_{10} and the ratio of the former with the measured phase speed c_p, U_{10}/c_p. For example, $u_* = 0.44\ m.s^{-1}$ and $h = 0.32\ m$ gives $\delta = 2.7$ and $\theta_{fd} = 1.55$, which gives a small relative error regarding (50). All the points give (δ, θ_{fd}) coordinates close to the theoretical limit.

3   A nonlinear Miles' approach

In this section we consider the air/water system from quasi-linear point of view in the sense that the water dynamics is considered nonlinear and irrotational but the airflow is kept linear . We use the β-Miles parameter as given by Eq. 43. In Miles's theory of wave generation [5,30], the complex air pressure P_a can be separated into two components, one in phase and one in quadrature with the free surface η. A phase shift between those two quantities is necessary to transfer energy from the air flow to the wave field. The transfer is only due to the part of P_a in quadrature with η. Hence, we will deal only with the acting pressure component, that is

$$P_a(x,t) = \rho_a \beta U_1^2 \eta_x(x,t), \tag{56}$$

3.1   The anti-diffusive nonlinear Schrödinger equation in finite depth

Let us consider the air/water system from a *quasi-linear* point of view i.e., the water dynamics is considered nonlinear and irrotational and, as in Miles' theory, the air flow
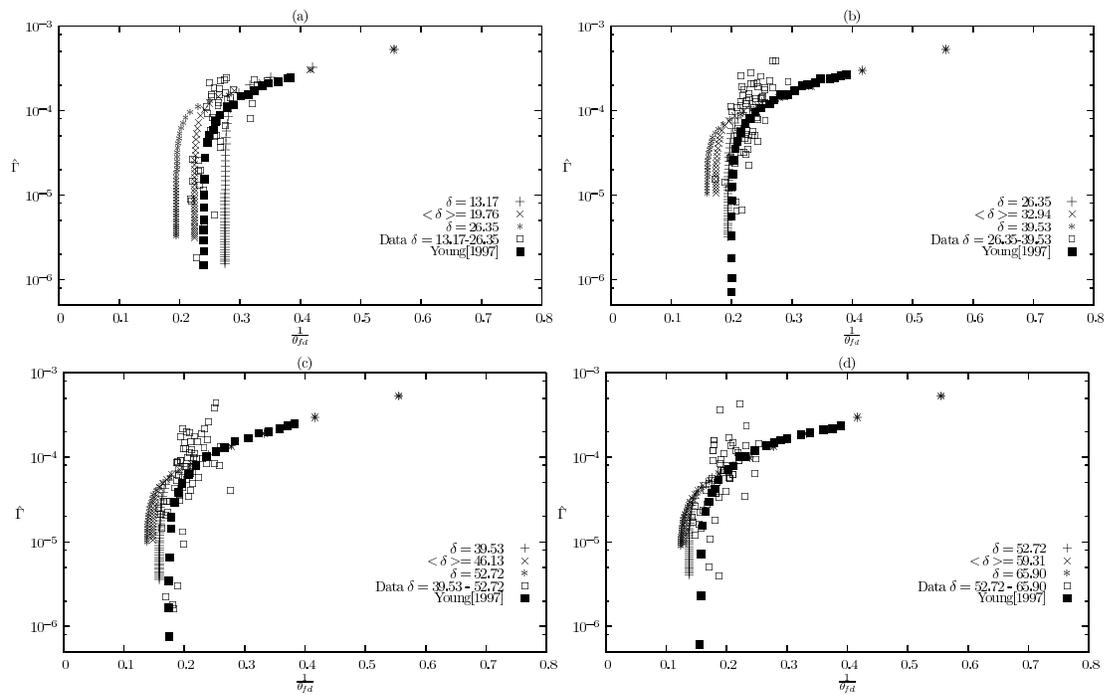
Figure 4. Growth rate $\hat{\Gamma}$ as a function of inverse wave age $1/\theta_{fd}$ for several values of the parameter δ. White squares correspond to Lake George experiment data, Black squares correspond to the empirical relationship (eq. (6)) in [23]. Present results correspond to symbols $+$, $\times$ and $*$. a: the dataset covers a range of wind speed corresponding to $\delta_Y = 0.1-0.2$, or using (48) $\delta = 13.17-26.35$, and an average value $< \delta >= (13.17 + 26.35)/2$ is used. b: same as "a" with $\delta_Y = 0.2-0.3$. c: same as "a" with $\delta_Y = 0.3-0.4$. d : same as "a" with $\delta_Y = 0.4-0.5$.
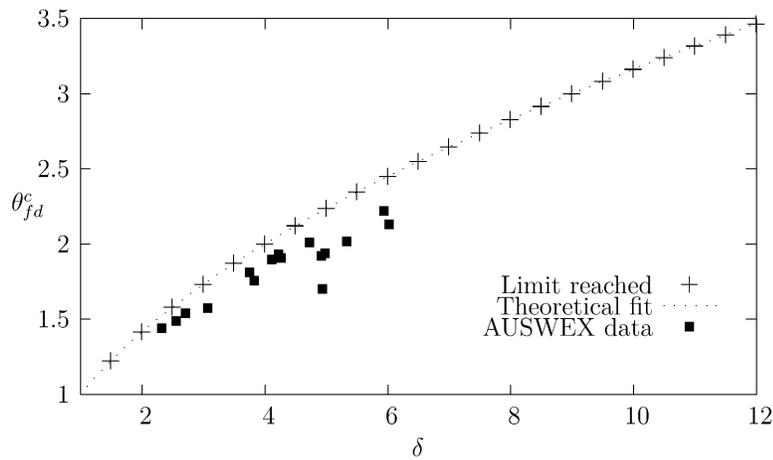

Figure 5. Parameter curves corresponding to zero growth rate. The theoretical limit is given by (50). The AUSWEX data are experimental results from [25] (the sea state is fairly close to the finite depth full development).

is kept linear. So with this assumption the complete irrotational Euler equations and boundary conditions in terms of the velocity potential $\phi(x, z, t)$ are

$$\phi_{xx} + \phi_{zz} = 0 \quad \text{for} \quad -h \le z \le \eta, \tag{57}$$

$$\phi_z = 0 \quad \text{for} \quad z = -h, \tag{58}$$

$$\eta_t + \phi_x \eta_x - \phi_z = 0 \quad \text{for} \quad z = \eta, \tag{59}$$

$$\phi_t + \frac{1}{2}\phi_x^2 + \frac{1}{2}\phi_z^2 + g\eta = -\frac{1}{\rho_w}P_a \quad \text{for} \quad z = \eta. \tag{60}$$

Using (56) the modified Bernoulli equation reads

$$\phi_t + \frac{1}{2}\phi_x^2 + \frac{1}{2}\phi_z^2 + g\eta = -s\beta U_1^2 \eta_x \quad \text{for} \quad z = \eta. \tag{61}$$

From equations (57), (58), (59) and (61) we find a wind-forced finite depth NLS equation for η as a function of the standard slow space and time variables $\xi = \varepsilon(x - c_g t)$ and $\nu = \varepsilon^2 t$, ($\varepsilon \ll 1$) and c_g the group velocity. The perturbed NLS equation reads

$$i\eta_\nu + a\eta_{\xi\xi} + b|\eta|^2\eta = id\eta \tag{62}$$

with c_g, a, b and d given by

$$c_g = \frac{c}{2}[1 + 2kh/\sinh(2kh)],$$

$$a = -\frac{c_g^2 - gh[1 - khT(1 - T^2)]}{2\omega},$$

$$b = \frac{k^4 c^2}{4\omega T^2}\left[\frac{9}{T^2} - 12 + 13T^2 - 2T^4 - \frac{2[2c + c_g(1 - T^2)]^2}{gh - c_g^2}\right],$$

$$d = s\frac{\beta}{2}\frac{U_1^2}{c^2}T\omega.$$

For more information about the derivation of the coefficients a and b see [31]. To derive a dimensionless wind-forced NLS equation we use (40) and we obtain in the original laboratory variables x and t (after a Galilean transformation in order to eliminate the linear term $c_g \eta_x$ and dropping the hats)

$$i\eta_t + A\eta_{xx} + B|\eta|^2\eta = iD\eta \tag{63}$$

with $c_g, A, B,$ and D now given by

$$c_g = \frac{1}{2\theta_{fd}}\left[1 + \frac{\delta}{\theta_{dw}^2}\frac{1 - T^2}{T}\right],$$

$$A = -\frac{c_g^2 - \delta[1 - \delta\theta_{dw}^{-2}(1 - T^2)]}{2\theta_{fd}\theta_{dw}^2},$$

$$B = \frac{1}{4T^2\theta_{fd}^3\theta_{dw}^2}\left[\frac{9}{T^2} - 12 + 13T^2 - 2T^4 - \frac{2[2\theta_{fd}^{-1} + c_g(1 - T^2)]^2}{\delta - c_g^2}\right],$$

$$D = s\frac{\beta}{2}\frac{T^{1/2}}{\theta_{dw}^3}.$$

Eq. (63) is a wind-forced finite depth NLS equation in dimensionless variables.

3.2 The Akhmediev, Peregrine and Ma solutions for weak wind inputs in finite depth

The wind-forced nonlinear Schrödinger equation allows the study of the wind influence on the freak waves dynamics [32–35]. Previous authors have carried out such studies in deep water. The present work allows, similar studies in finite depth with the right Miles' growth rates. In the following we are going only to consider the so called focusing NLS equation i.e., positive A and B. Introducing η' and x' as

$$\eta' = \sqrt{B}\eta, \quad x' = \frac{x}{\sqrt{A}},$$

Dropping the primes, Eq. (63) becomes

$$i\eta_t + \eta_{xx} + |\eta|^2\eta = iD\eta. \tag{64}$$

Introducing a function $M(x,t)$ as

$$M(x,t) = \eta(x,t)\exp(-Dt), \tag{65}$$

we obtain from (64)

$$iM_t + M_{xx} + \exp(2Dt)|M|^2M = 0. \tag{66}$$

In order to reduce Eq. (64) into the standard form of the NLS with constant coefficients we proceed in the following way. First of all we consider the wind forcing $(2Dt)$ to be weak, such that the exponential can be approximated by $\exp(2Dt) \sim 1 + 2Dt$ so

$$iM_t + M_{xx} + n|M|^2M = 0, \quad n = n(t) = 1 - 2Dt. \tag{67}$$

Now with a change of coordinates from (x,t) to (z,τ) defined by

$$z(x,t) = xn(t), \quad \tau(x,t) = xn(t), \tag{68}$$

and scaling the wave envelope as [35]

$$M(z,\tau) = \Psi(z,\tau)\sqrt{n(\tau)}\exp\left(\frac{-iDz^2}{n(\tau)}\right), \tag{69}$$

we reduce (67) to the standard focusing equation

$$i\Psi_\tau + \Psi_{xx} + |\Psi|^2\Psi = 0. \tag{70}$$

Equation (70) admits well known breather solutions that are simple analytical prototypes for rogue wave events. They are the Akhmediev (Ψ_A) [36], the Peregrine (Ψ_P) [37] and the Kuznetsov-Ma (Ψ_M) [38] breather solutions. [39] investigated whether freak waves in deep water could be modeled by Ψ_A, Ψ_P or by Ψ_M. [35] considered the influence of weak wind forcing and dissipation on these Ψ_A, Ψ_P or Ψ_M solutions in deep water. The present work allows us to exhibit expressions for Ψ_A, Ψ_P and Ψ_M *under the influence of weak*

wind forcing in finite depth h given by the extended Miles mechanism. These solutions read [39]:

$$\eta_A = P(\tau)\{\frac{\cosh(\Omega\tau - 2i\omega) - \cos(\omega)\cos(pz)}{\cosh(\Omega\tau) - \cos(\omega)\cos(pz)}\}, \tag{71}$$

with $p = 2\sin(\omega)$, $\Omega = 2\sin(2\omega)$ ω real and p related to the spatial period $2\pi/p$

$$\eta_P = P(\tau)\{1 - \frac{4(1 + 4i\tau)}{1 + 4z^2 + 16\tau^2}\}, \tag{72}$$

$$\eta_M = P(\tau)\{\frac{\cos(\Omega\tau - 2i\omega) - \cosh(\omega)\cosh(pz)}{\cosh(\Omega\tau) - \cos(\omega)\cos(pz)}\}, \tag{73}$$

where $p = 2\sinh(\omega)$, $\Omega = 2\sinh(2\omega)$ and Ω real and related to the time period $2\pi/\Omega$ and

$$P(\tau) = n(\tau)\exp\left[\frac{-iDz^2}{n(\tau)}\right]\exp\left[2i\tau\right].$$

It is worth noticing that many works are done on Akhmediev solutions and rogue waves. We can mention here one of the recent works of Grinevich and Santini [40] and references therein.

4 The Nonlinear Jeffrey's approach

Jeffreys introduced a second significant mechanism, extensively researched today, in 1925. The principle was that waves if sufficiently disrupted, could break the continuity of the airflow and induce a gradient of pressure. This understanding could have practical implications, allowing the wave to grow quickly according to the relative distance between the phase speed of the wave and the wind speed. Jeffreys found the main idea behind this mechanism by analogizing it with a sphere immersed in a laminar fluid flow. Jeffreys noticed that, in the viscous case, the fluid particles do not do everything around the sphere. Those hitting the forehead slide on the sphere and take off shortly after the halfway point, and on the other side, an area is almost stagnant and has a relative speed relative to the sphere close to zero. (1925) When a wave is large enough, it breaks the continuity of the airflow, and a horizontal axis vortex forms on the side sheltered from the wind by the wave. Other smaller whirlpools form between the large vortex and the laminar flow. This phenomenon, called airflow separation, has been observed in waves, see Figure (6). In this case, the face of the wave opposing the wind will experience greater pressure, and the sheltered side will experience less pressure. This gradient induces a reaction at the surface level.

4.1 The Nonlinear Serre-Green-Naghdi Approximation

We associated water particles, in a system of two-dimensional Cartesian coordinates (x, z) with origin 0, where z is the upward vertical direction. We let $z = 0$ at the water–air interface. Hence, the positive values of z, $z \in\ ]0, \infty[$, correspond to the (unperturbed)
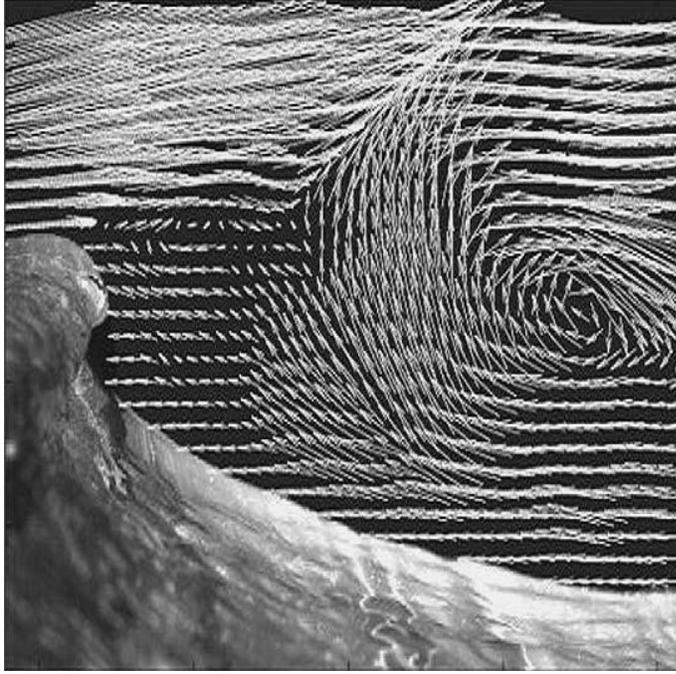
Figure 6. Jeffreys' mechanism - Airflow separation observed by "Particle Image Velocimetry" over a breaking wave [41]. The air pressure on the windward face of the wave is larger than the leeward face, which is the origin of continuous energy transfer from wind to wave.

air domain, while negative values of z, $z \in [-h, 0]$ correspond to the (unperturbed) water domain. Consequently, for the bottom of the water domain of depth h, we obtain $z = -h$. The bottom is considered to be impermeable, and both water and air, are taken to be inviscid and incompressible. Moreover, the surface tension effects, at the interface, are not taken into account. The governing equations are the well known Euler equations, with the mass conservation equations used in (x, z, t) frame, where t accounts for the time. Namely,

$$u_x + w_z = 0, \tag{74a}$$

$$\rho_w(u_t + uu_x + wu_z) = -P_x, \tag{74b}$$

$$\rho_w(w_t + uw_x + ww_z) = -P_z - g\rho_w, \tag{74c}$$

where $u(x, z, t)$ and $w(x, z, t)$ are the fluid's horizontal and vertical velocities, respectively. $P(x, z, t)$ is the Archimedean pressure, g the gravitational acceleration, ρ_w is the water density and subscripts x, z and t denote partial derivatives with respect to x, z and t, respectively. The set of Equations (74) are completed by the following boundary conditions:

$$w = 0, \quad \text{at} \quad z = -h, \tag{75a}$$

$$\eta_t + u\eta_x - w = 0, \quad \text{at} \quad z = \eta, \tag{75b}$$

$$P = P_a, \quad \text{at} \quad z = \eta, \tag{75c}$$

where $P_a(x, z, t)$ is the air pressure, and Equation (75c) expresses the pressure's continuity across the air/water interface. Notice that $z = \eta(x, t)$ is the perturbed water surface. For convenience, we introduced a reduced pressure $\mathbf{P}$, such that $\mathbf{P}(x, z, t) = P(x, z, t) + \rho_w gz - P_0$, where P_0 denotes the atmospheric pressure. Using the reduced pressure $\mathbf{P}(x, z, t)$, the set of Equations (74) can be written as follows:

$$\rho_w(u_t + uu_x + wu_z) = -\mathbf{P}_x, \tag{76a}$$

$$\rho_w(w_t + uw_x + ww_z) = -\mathbf{P}_z, \tag{76b}$$

$$\mathbf{P}(x, \eta, t) - \rho_w g\eta + P_0 = P_a(x, \eta, t). \tag{76c}$$

Shallow water model equations, such as the Korteweg-Vries, modified Korteweg-Vries, and Boussinesq equations and many others, are usually derived by performing an asymptotic analysis directly from the equations of continuity (74a), the motion Equations (3a,b) and the boundary conditions (2a,b) and (76c) (see [9] and references therein). In this work, our approach was somewhat different, in the sense that instead of applying a perturbation theory to the entire problem, we first considered the nonlinear evolution of a given velocity field profile. Indeed, we assumed the horizontal velocity $u(x, z, t)$ to be independent of z, i.e.,

$$u = u(x, t). \tag{77}$$

The choice of Equation (77), is known as the *columnar flow hypothesis*, which was introduced by [42], and [43]. Using Equations (74a), (75a) and (77) we obtain

$$w(x, z, t) = -(z + h)u_x(x, t). \tag{78}$$

Hence, Equations (75b) and (3a,b) read

$$\eta_t + [u(\eta + h)]_x = 0, \tag{79a}$$

$$\rho_w(u_t + uu_x) = -\mathbf{P}_x, \tag{79b}$$

$$\rho_w(z + h)(u_{xt} + uu_{xx} - u_x^2) = \mathbf{P}_z. \tag{79c}$$

The integration of Equation (79c), using Equation (76c), yields the pressure $\mathbf{P}(x, z, t)$:

$$\mathbf{P}(x, z, t) = \frac{1}{2}\rho_w[(z + h)^2 - (\eta + h)^2](u_{xt} + uu_{xx} - u_x^2) + P_a(x, \eta, t) + \rho_w g\eta - P_0. \tag{80}$$

The next step consists of substituting Equation (80) in Equation (79b), and taking the z-average of Equation (79b) for $-h \leq z \leq \eta$. Finally, using Equation (76c) we obtained the following system:

$$\eta_t + [u(\eta + h)]_x = 0, \tag{81a}$$

$$u_t + uu_x + g\eta_x - \frac{1}{3(\eta + h)}\{(\eta + h)^3(u_{xt} + uu_{xx} - u_x^2)\}_x = -\frac{1}{\rho_w}[P_a(x, \eta, t]_x. \tag{81b}$$

If $P_a = P_0$, Equations (8a,b) are reduced to the usual Serre–Green–Naghdi equations. However, in our approach, P_a was not taken as equal to P_0, and the expression of $P_a(x, z, t)$ was found using the sheltering mechanism.

4.2 Jeffreys' Sheltering Mechanism of Wind Waves Generation Applied to Serre-Green-Nagdhi Equations

The physical sheltering mechanism assumes that the energy transfer is caused by pressure drag (also known as "form drag"). The air pressure on the windward face of the wave is larger than the leeward face, which is the origin of continuous energy transfer from wind to wave. Using dimensional arguments, Jeffreys [2, 3] showed that the air pressure perturbation $P_a(x, z, t)$ evaluated on the surface can be represented by

$$P_a(x, z = \eta, t) = \rho_a \epsilon (U_{10} - c)^2 \eta_x(x, t), \tag{82}$$

where ϵ is the *sheltering coefficient*, ρ_a is the air density and U_{10} is the wind velocity at a 10 m height. The sheltering coefficient is less than 1 ($\epsilon < 1$). By substituting Equation (82) in Equation (81b), we obtained

$$\eta_t + [u(\eta + h)]_x = 0, \tag{83a}$$

$$u_t + uu_x + g\eta_x - \frac{1}{3(\eta + h)}\{(\eta + h)^3(u_{xt} + uu_{xx} - u_x^2)\}_x = -\epsilon s \Delta^2 \eta_{xx}, \tag{83b}$$

where $s = \frac{\rho_a}{\rho_w} \sim 10^{-3}$ and $\Delta = (U_{10} - c)$. Thus, Equation (83) constitutes the fully non-linear Serre–Green–Naghi system describing surface wave propagation in shallow water under the action of the wind sheltering mechanism.

For convenience, we introduced new variables $S(x, t)$, $U(x, t)$ and α, defined as follows:

$$S(x, t) = \eta(x, t) + h, \tag{84a}$$

$$U(x, t) = u(x, t), \tag{84b}$$

$$\alpha = \epsilon \Delta^2. \tag{84c}$$

Using the variables (84), the system of Equation (10a,b) can be written as follows:

$$S_t + U_x S + U S_x = 0, \tag{85a}$$

$$U_t + UU_x + gS_x - \frac{1}{3S}\left\{S^3\left[U_{xt} + UU_{xx} - (U_x)^2\right]\right\}_x = -\alpha s S_{xx}. \tag{85b}$$

Considering the following frame σ, and the slow time τ:

$$\sigma = x - vt, \tag{86a}$$

$$\tau = st, \tag{86b}$$

and applying Leibniz's chain rules by considering the change of variables (86), the x and t derivatives can be expressed as follows:

$$\partial_x = \partial_\sigma, \quad \partial_t = -v\partial_\sigma + s\partial_\tau, \quad \partial_{xt}^2 = -v\partial_{\sigma\sigma}^2 + s\partial_{\tau\sigma}^2, \quad \partial_{xx} = \partial_{\sigma\sigma}, \quad \partial_{xxx} = \partial_{\sigma\sigma\sigma}. \tag{87}$$

With the parameter s being small ($s \sim 10^{-3}$), Equation (12a,b) can be expanded in terms of s, as follows:

$$U = U_0 + sU_1 + O(s^2), \tag{88a}$$

$$S = S_0 + sS_1 + O(s^2). \tag{88b}$$

Notice that the expansion should not be continued beyond the first order, because Equation (85b) is an s^1-order equation. Using the partial derivate chain rules (87) in the SGN Equation (85) yields the following:

At order 0

$$-vS_{0,\sigma} + U_{0,\sigma}S_0 + U_0 S_{0,\sigma} = 0, \tag{89a}$$
$$-vU_{0,\sigma} + U_0 U_{0,\sigma} + gS_{0,\sigma} + S_0 S_{0,\sigma}\left[vU_{0,\sigma\sigma} - U_0 U_{0,\sigma\sigma} + (U_{0,\sigma})^2\right]$$
$$+ \frac{1}{3}(S_0)^2\left[vU_{0,\sigma\sigma\sigma} - U_0 U_{0,\sigma\sigma\sigma} + U_{0,\sigma}U_{0,\sigma\sigma}\right] = 0. \tag{89b}$$

At order 1

$$-vS_{1,\sigma} + U_{0,\sigma}S_1 + U_{1,\sigma}S_0 + U_0 S_{1,\sigma} + U_1 S_{0,\sigma} = -S_{0,\tau}, \tag{90a}$$
$$-vU_{1,\sigma} + U_0 U_{1,\sigma} + U_1 U_{0,\sigma} + gS_{1,\sigma} + (S_0 S_{1,\sigma} + S_1 S_{0,\sigma})\left[vU_{0,\sigma\sigma} + (U_{0,\sigma})^2 - U_0 U_{0,\sigma\sigma}\right]$$
$$+ S_0 S_{0,\sigma}\left[vU_{1,\sigma\sigma} - U_0 U_{1,\sigma\sigma} - U_1 U_{0,\sigma\sigma} + 2U_{0,\sigma}U_{1,\sigma}\right]$$
$$+ \frac{1}{3}(S_0)^2\left[vU_{1,\sigma\sigma\sigma} - U_0 U_{1,\sigma\sigma\sigma} - U_1 U_{0,\sigma\sigma\sigma} + U_{0,\sigma}U_{1,\sigma\sigma} + U_{1,\sigma}U_{0,\sigma\sigma}\right]$$
$$+ \frac{2}{3}S_1 S_0\left[vU_{0,\sigma\sigma\sigma} + U_{0,\sigma}U_{0,\sigma\sigma} - U_0 U_{0,\sigma\sigma\sigma}\right] = -\alpha S_{0,\sigma\sigma} - U_{0,\tau} - \frac{1}{3}(S_0)^2 U_{0,\tau\sigma\sigma} + S_0 S_{0,\sigma}U_{0,\tau\sigma}. \tag{90b}$$

The set of Equations (89) and (90) can be reformulated in a matrix. Indeed, Equation (89) can be written equivalently as follows:

$$\begin{pmatrix} \widehat{A}_0 & \widehat{B}_0 \\ \widehat{C}_0 & \widehat{D}_0 \end{pmatrix} \begin{pmatrix} U_0 \\ S_0 \end{pmatrix} = \begin{pmatrix} 0 \\ 0 \end{pmatrix}, \tag{91}$$

where

$$\widehat{A}_0 = S_0 \partial_\sigma, \tag{92a}$$
$$\widehat{B}_0 = -v\partial_\sigma + U_0 \partial_\sigma, \tag{92b}$$
$$\widehat{C}_0 = -v\partial_\sigma + U_0 \partial_\sigma + \frac{1}{3}(S_0)^2\left[v\partial_{\sigma\sigma\sigma} - U_0\partial_{\sigma\sigma\sigma} + U_{0,\sigma}\partial_{\sigma\sigma}\right], \tag{92c}$$
$$\widehat{D}_0 = g\partial_\sigma + \left[vU_{0,\sigma\sigma} - U_0 U_{0,\sigma\sigma} + (U_{0,\sigma})^2\right]S_0\partial_\sigma. \tag{92d}$$

Similarly, Equation (90) can be expressed as follows:

$$\begin{pmatrix} \widehat{A}_1 & \widehat{B}_1 \\ \widehat{C}_1 & \widehat{D}_1 \end{pmatrix} \begin{pmatrix} U_1 \\ S_1 \end{pmatrix} = \begin{pmatrix} E_1 \\ E_2 \end{pmatrix}, \tag{93}$$

where

$$\widehat{A}_1 = S_0\partial_\sigma + S_{0,\sigma}, \tag{94a}$$

$$\widehat{B}_1 = -v\partial_\sigma + U_0\partial_\sigma + U_{0,\sigma}, \tag{94b}$$

$$\widehat{C}_1 = -v\partial_\sigma + U_0\partial_\sigma + U_{0,\sigma} + S_0 S_{0,\sigma}\left[v\partial_{\sigma\sigma} - U_0\partial_{\sigma\sigma} - U_{0,\sigma\sigma} + 2U_{0,\sigma}\partial_\sigma\right]$$
$$+ \frac{1}{3}(S_0)^2\left[v\partial_{\sigma\sigma\sigma} - U_0\partial_{\sigma\sigma\sigma} - U_{0,\sigma\sigma\sigma} + U_{0,\sigma}\partial_{\sigma\sigma} + U_{0,\sigma\sigma}\partial_\sigma\right], \tag{94c}$$

$$\widehat{D}_1 = g\partial_\sigma + \left[vU_{0,\sigma\sigma} - U_0 U_{0,\sigma\sigma} + (U_{0,\sigma})^2\right](S_0\partial_\sigma + S_{0,\sigma})$$
$$+ \frac{2}{3}S_0\left[vU_{0,\sigma\sigma\sigma} - U_0 U_{0,\sigma\sigma\sigma} + U_{0,\sigma}U_{0,\sigma\sigma}\right], \tag{94d}$$

$$E_1 = -S_{0,\tau}, \tag{94e}$$

$$E_2 = -\alpha S_{0,\sigma\sigma} - U_{0,\tau} + \frac{1}{3}(S_0)^2 U_{0,\tau\sigma\sigma} + S_0 S_{0,\sigma}U_{0,\tau\sigma}. \tag{94f}$$

4.3   Application of Green's Theorem in One Dimension

Green's theorem in one dimension has been proved and applied to linear differential operators [44–46]. Here, by extension, we applied this theorem to matrix differential operators. To do so, we briefly recalled the following theorem:

$$\int_a^b \left[zP(y) - y\bar{P}(z)\right]dx = [P(y,z)]_a^b, \tag{95}$$

where P is a linear differential operator and y and z, any two functions of x and, $\bar{P}(z)$ and $P(y,z)$, are the adjoint and the bilinear differential expressions of $P(y)$, respectively [47]. This theorem, in its usual form, as it is shown in (95), was previously used to show the damping of solitary waves [48, 49].

In our case, we considered operators $\widehat{L}_0$ and $\widehat{L}_1$, defined as follows:

$$\widehat{L}_0 = \begin{pmatrix} \widehat{A}_0 & \widehat{B}_0 \\ \widehat{C}_0 & \widehat{D}_0 \end{pmatrix}, \qquad \widehat{L}_1 = \begin{pmatrix} \widehat{A}_1 & \widehat{B}_1 \\ \widehat{C}_1 & \widehat{D}_1 \end{pmatrix}.$$

Using $\widehat{L}_0$ and $\widehat{L}_1$, Equations (91) and (93) become

$$\widehat{L}_0 V_0 = 0 \quad \text{and} \quad \widehat{L}_1 V_1 = E, \tag{96}$$

where

$$V_0 = \begin{pmatrix} U_0 \\ S_0 \end{pmatrix}, \qquad V_1 = \begin{pmatrix} U_1 \\ S_1 \end{pmatrix}, \qquad E = \begin{pmatrix} E_1 \\ E_2 \end{pmatrix}.$$

Taking into account the symmetric behaviour of $S(x,t)$ and $U(x;t)$ at $x = \pm\infty$, the extension of Green's theorem in one dimension to linear differential matrix operator $\widehat{L}_1$ yields

$$\int_{-\infty}^{+\infty}\left(V_0^\dagger \widehat{L}_1 V_1 - V_1^\dagger \widehat{L}_1 V_0\right)d\sigma = 0, \tag{97}$$

where $V_0^\dagger$ and $V_1^\dagger$ are V_0 and V_1 transposed, respectively. This extension can easily be proved following the procedure proposed in the original work of [44].

4.4   Blow-Up in Finite Time of the Serre-Green-Naghdi Soliton Solution

Using Equations (96) and (97), we have:

$$\int_{-\infty}^{+\infty}\left[-U_0 S_{0,\tau} + S_0\left(-\alpha S_{0,\sigma\sigma} - U_{0,\tau} + \frac{1}{3}(S_0)^2 U_{0,\tau\sigma\sigma} + S_0 S_{0,\sigma} U_{0,\tau\sigma}\right)\right]d\sigma = 0, \quad (98)$$

which can be written as follows:

$$-\int_{-\infty}^{+\infty}\left[\frac{\partial}{\partial\tau}(U_0 S_{0,})\right]d\sigma + \alpha\int_{-\infty}^{+\infty}(S_{0,\sigma})^2 d\sigma - \alpha\left[S_0 S_{0,\sigma}\right]_{-\infty}^{+\infty} + \left[\frac{1}{3}(S_0)^3 U_{0,\tau\sigma}\right]_{-\infty}^{+\infty} = 0, \quad (99)$$

where U_0 and S_0 are the unperturbed solutions with a time-dependent amplitude, namely,

$$U_0 = c_0\left(1 + \frac{a(\tau)}{h}\right)^{1/2}\left(1 - \frac{h}{S_0}\right), \quad (100)$$

$$S_0 = \frac{a(\tau)}{[\cosh(\beta)]^2}, \qquad \beta = \sqrt{\frac{3}{4}}\left(\frac{1}{h}\right)\left(\frac{a(\tau)}{a(\tau) + h}\right)^{1/2}\left[x - c_0 t\left(1 + \frac{a(\tau)}{h}\right)^{1/2}\right]. \quad (101)$$

After inserting (101) and (100) into Equation (99), alongside Equation (86) it can be noticed that the limit of $\dfrac{1}{\cosh(\sigma)}$ tends to zero, while $\sigma \to \pm\infty$. The Equation (99) yields the following:

$$\int_{a(0)}^{a(\tau)}\frac{(a+h)^{1/2}(2a+h)}{a^3}da = \frac{4\alpha}{5c_0}\left(\frac{1}{h}\right)^{3/2}\tau. \quad (102)$$

Using the variable r, Equation (102) yields:

$$\int_{r(0)}^{r(\tau)}\frac{(1+r)^{1/2}(1+2r)}{r^3}dr = \frac{4\alpha}{5c_0 h}\tau. \quad (103)$$

The series expansion for a small value of r in the Equation yields:

$$\int_{r(0)}^{r(\tau)}\left(\frac{1}{r^3} + \frac{5}{2r^2} + \frac{7}{8r} - \frac{3}{16} + o(r)\right)dr = \frac{4\alpha}{5c_0 h}\tau. \quad (104)$$

After integration, Equation (104) becomes

$$\left[-\frac{3r}{16} + \frac{7\ln(r)}{8} - \frac{5}{2r} - \frac{1}{2r^2} + o(r^2)\right]_{r(0)}^{r(\tau)} = \frac{4\alpha}{5c_0 h}\tau, \quad (105)$$

and by keeping the leading term for r small, Equation (105) becomes

$$\left[-\frac{1}{2r^2}\right]_{r(0)}^{r(\tau)} = \frac{4\alpha}{5c_0 h}\tau. \quad (106)$$

Hence, the time dependent amplitude reads as follows:

$$a(\tau) = \frac{A_0}{\sqrt{1 - \dfrac{8\alpha A_0^2\tau}{5c_0 h^3}}}, \quad (107)$$

where $A_0 = a(0)$. From Eq. (107), it can be seen that the amplitude $a(\tau)$ tends to infinity, when the slow time τ approaches a certain value τ_b, which we call the *"slow" blow-up time*. Replacing $\alpha = \epsilon \Delta^2$, and $\tau = st$, the blow-up time can be written as follows:

$$t_b = \frac{5c_0 h^3}{8\epsilon \Delta^2 A_0^2 s}, \tag{108}$$

where $\Delta^2 = (U_{10} - C_{GN})^2$, and the dispersion relation of the SGN solitary wave C_{GN}, can be written [10, 50] as follows:

$$C_{GN} = \frac{c_0}{\sqrt{1 + \frac{1}{3}(kh)^2}}. \tag{109}$$

4.5   Blow-up Time's Effective evaluation

In order to effectively evaluate the blow-up time t_b and the growth rate of wind waves in finite depth, we used detailed measurements of shallow water parameters in finite depth experiments conducted in the IRPHÉ/Pythéas wind-wave tank [51]. These measurements were carried out for non-dimensional depth kh and non-dimensional initial waves' peak value kA_0. This led us to consider the non-dimensional soliton-like solution (a solution which at any time looks exactly as a soliton but with parameters which are triggered by the interaction with the source) kS_0, instead of S_0, as well as the non-dimensional amplitude ka that we denoted as a function of non dimensional time $\bar{t}$, as follows:

$$ka(\bar{t}) = \frac{kA_0}{\sqrt{1 - \frac{8\epsilon(kA_0)^2 s}{5(kh)^2}\bar{t}}}, \tag{110}$$

where

$$\bar{t} = \frac{\Delta^2}{c_0 h} t. \tag{111}$$

Notice that the values of c_0 as well as U_{10} were also measured experimentally. For this reason, in what follows, the values of c_0 differ slightly from the theoretical values $c_0 = \sqrt{gh}$.

Using the experimental data of IRPHÉ/Pythéas facilities ([51]), for

$$h = 0.14 \text{ m}, \quad kh = 1.54, \quad kA_0 = 0.114, \quad c_0 = 0.92 \text{ m/s}, \quad U_{10} = 4.82 \text{ m/s}, \tag{112}$$

for the sheltering coefficient, we used $\epsilon = 0.5$, and for the small parameter we used $s = 0.001$. Using experimental data (112) and Equations (108) and (109) assisted in calculating the value of the blow-up time:

$$t_b \approx 1721 \text{ s.} \tag{113}$$

The x-position of the SGN soliton-like solution as a function of time is found using

$$x(t) = c_0 t \left(1 + \frac{a(\tau)}{h}\right)^{1/2}. \tag{114}$$

Table 1. The growth rate of the SNG solitary wave at different times and positions, for depth $h = 0.14$ m, and wind speed of 10 m $U_{10} = 4.82$ m/s.

t (s)	0	40	...	750	1000	1250	1400
x (m)	0	35	...	722	972	1229	1329
growth rate		0.09	...	0.15	0.55	1	1.36

Table 2. The growth rate of the SNG solitary wave at different times and positions, for depth $h = 0.26$ m, and wind speed at 10 m $U_{10} = 4.35$ m/s.

t (s)	0	40	...	750	1000	1250	15,000
x (m)	0	41	...	772	1030	1288	1547
growth rate		0.02	...	0.06	0.08	0.1	0.12

The length of the IRPHÉ/Pythéas wind–wave tank facility was 40 m. The growing solitary wave reaches the tank's end after 40–45 s. Consequently, the wave amplitude is not nearly that of the blow-up. The growth rate of the solitary wave at different times and positions, for $h = 0.14$ m, and $U_{10} = 4.48$ m/s, is given in (Table 1). In these conditions, when the wave reaches the tunnel's end, the growth rate is approximately 0.1. Hence, it is at the measurability limit of the IRPHÉ/Pythéas wind–wave tank facility.

And for

$$h = 0.26 \text{ m}, \quad kh = 2.57, \quad kA_0 = 0.146, \quad c_0 = 1.0 \text{ m/s}, \quad U_{10} = 4.35 \text{ m/s}, \quad (115)$$

with a sheltering coefficient $\epsilon = 0.5$ and small parameter $s = 0.001$. Similarly, experimental data (115) and Equations (108) and (109) led to the corresponding blow-up time:

$$t_b \approx 7008 \text{ s.} \tag{116}$$

The continuous growth of (kS_0), leads to blow-up at finite time, $t_b \approx 7008$ s, which of course, is out of reach. Therefore, in this case, a significant growth in the solitary wave's amplitude was not observable in experimental facilities, but it could be *in situ*. The growth rate of the solitary wave solution at different times and positions, for $h = 0.26$ m, and $U_{10} = 4.35$ m/s, is given in (Table 2).

5   Korteweg-de Vries-Burger equation

The Jeffreys' theory allows to compute the linear wave growth of wind-generated normal Fourier modes of wave-number k. The physical mechanism behind is "focusing", in the sense that energy passes continuously from the air to the surface wave. Consequently the wave amplitude $\eta(x, t, k)$ (x space and t time) grows exponentially in time i.e.; $\eta(x, t, k) \sim \exp{(\gamma_J t)}$ more or less quickly according to the coefficient γ_J, which depends on the wind speed and the water depth h. Once the linear and dispersionless approximation breaks down, non-linear and dispersive processes begin to play a role. So the issue addressed here is: "how to describe the evolution in time of a normal mode k, under the

competing actions of (weak) nonlinearity, dispersion and anti-dissipation in the sense of a contiuous energy transfer from wind to water?" Nonlinearity is likely to balance dispersive effects, or to stop exponential decay or growth of wave amplitude in time due to dissipation or "anti-dissipation". Equilibrium between nonlinearity and dispersion can evolve in time to form solitary waves as in the Korteweg-de Vries equation [52, 53]. Balance between dissipation or "anti-dissipation" and nonlinearity creates shock structures as in the Burgers equation [52]. The standard equation describing competition between weak non-linearity, dispersion and dissipation is the KdV-B equation. It appears in many physical contexts [54–59]. In this section, in order to study simultaneous competing effects of weakly nonlinearity, dispersion and "anti-dissipation" we derive a KdV-B type equation with *dissipation turned into "anti-dissipation"*.

Green-Naghdi equations under the wind action [10, 50, 60] are given by Eqs (83a) and (83b). We introduce dimensionless "primed" variables, x', t' and η' as follows:

$$x = \lambda_0 x', \qquad t = \frac{\lambda_0}{c_0} t', \qquad \eta = a_0 \eta', \tag{117}$$

where $c_0 = (gh)^{1/2}$, a_0 and λ_0 are initial typical wave amplitude and wavelength, respectively. In addition, we define two fundamental parameters, commonly used in the classical water surface studies, namely, ν and δ, as follows:

$$\nu = \frac{a_0}{h}, \qquad \delta = \frac{h}{\lambda_0}. \tag{118}$$

Finally, in order to obtain the dimensionless, scaled Green-Naghdi equations of motion, the following scaling is required [55]:

$$u = \nu u_0. \tag{119}$$

Introducing Eqs (117), (118) and (119) in Eqs (83b) and (83a), we obtain the following dimensionless equations

$$u_{0,t} + \nu u_0 u_{0,x} + \eta_x = -\epsilon s \Delta^2 \delta \eta_{xx} + \frac{\delta^2}{3(1+\nu\eta)} \{(1+\nu\eta)^3 (u_{0,xt} + \nu u_0 u_{0,xx} - \nu u_{0,x}^2)\}_x, \tag{120a}$$

$$\eta_t + [u_0(1+\nu\eta)]_x = 0, \tag{120b}$$

where, for convenience, the "primes" of dimensionless quantities are omitted. Now, we consider a wave moving from left to right [52]. At the lowest order, by neglecting the terms of order ν and δ and any higher orders, Eqs (120a) and (120b) are reduced to

$$u_{0,t} + \eta_x = 0, \tag{121a}$$

$$\eta_t + u_{0,x} = 0. \tag{121b}$$

Eqs (121a) and (121b) are equivalent to

$$\eta_t + \eta_x = u_{0,t} + u_{0,x} = 0, \tag{122}$$

and its solution is

$$u_{0,x}(x,t) = \eta(x,t). \tag{123}$$

Now we look for a perturbed solution with follow form:

$$u_0 = \eta + \nu\mathbb{A} + \delta\mathbb{B} + \delta^2\mathbb{C} + O(\delta\nu, \delta^2\nu, \nu^2), \tag{124}$$

where $\mathbb{A}$, $\mathbb{B}$ and $\mathbb{C}$ are functions of η and its derivatives. Inserting Eq. (124) in (120a) and (120b), we obtain

$$\eta_t + \eta_x + \nu(\mathbb{A}_t + \eta\eta_x) + \delta(\mathbb{B}_t + \epsilon s\Delta^2\eta_{xx}) + \delta^2(\mathbb{C}_t - \frac{1}{3}\eta_{xxt}) + O(\delta\nu, \delta^2\nu, \nu^2) = 0, \tag{125a}$$

$$\eta_t + \eta_x + \nu(\mathbb{A}_x + \eta\eta_x) + \delta(\mathbb{B}_x + \delta^2\mathbb{C}_x + O(\delta\nu, \delta^2\nu, \nu^2) = 0, \tag{125b}$$

where

$$\eta_t = -\eta_x + O(\delta\nu, \delta^2\nu, \nu^2). \tag{126}$$

Therefore, in Eq. (125a), all the t-derivatives may be substituted by $-\partial_x$. Hence, Eqs (125a) and (125b) are compatible, if

$$\mathbb{A} = -\frac{1}{4}\eta^2, \qquad \mathbb{B} = \frac{1}{2}s\epsilon\Delta^2\eta_x, \qquad \mathbb{C} = \frac{1}{6}\eta_{xx}. \tag{127}$$

Substituting Eq. (127) in Eqs (125a) and (125b), yields

$$\eta_t + \eta_x + \frac{3}{2}\nu\eta\eta_x + \frac{\delta^2}{6}\eta_{xxx} + s\epsilon\frac{\delta}{2}\Delta^2\eta_{xx} = 0, \tag{128a}$$

$$u - \eta + \frac{\nu}{4}\eta^2 - s\epsilon\frac{\delta}{2}\Delta^2\eta_x - \frac{1}{6}\delta^2\eta_{xx} = 0. \tag{128b}$$

Eq. (128a) is the KdV-B equation, while Eq. (128b) is a Riemann invariant.

5.1   Solution of Korteweg-de Vries-Burger equation

In order to find the solution of Eq.(128a), we apply the following change of variables:

$$\sigma = x - t, \qquad t_1 = \delta^2 t. \tag{129}$$

Hence, Eq.(128a) becomes:

$$\eta_{t_1} + \frac{3}{2}\eta\eta_\sigma + \frac{\delta^2}{6\nu}\Delta^2\eta_{\sigma\sigma\sigma} + \frac{\delta}{2\nu}\Delta^2 s\eta_{\sigma\sigma} = 0. \tag{130}$$

It worth noticing that the limit of Eq. (130), as $s \to 0$, yields to the well known KdV equation:

$$\eta_{t_1} + \frac{3}{2}\eta\eta_\sigma + \frac{\delta^2}{6\nu}\Delta^2\eta_{\sigma\sigma\sigma} = 0. \tag{131}$$

This result is quite natural, since $s \to 0$, amounts to neglecting the action of the wind. Therefore, it is possible to assume that the solution KdV-B, Eq. (130), has the same form as the solution of Eq. (131), namely

$$\eta(\sigma, t_1) = \frac{a}{\cosh^2\left[P(\sigma - c't_1)\right]}. \tag{132}$$

This is the typical "soliton" solution of KdV equation, with one difference however, the amplitude a in Eq. (132) can be time-dependant, whereas the amplitude of KdV equation is not.

Inserting (132) in (130), we obtain

$$P = \sqrt{\frac{3\nu}{4\delta^2}}, \qquad c' = \frac{a}{2}. \tag{133}$$

Now, the task is to find the time-dependent expression of $a(t)$ in Eq. (132).

Noticing that the anti diffusive term $\dfrac{\delta}{2\nu}\Delta^2 s\eta_{\sigma\sigma}$ in Eq. (130), is of order δ^3 and small enough at $t = 0$, one can find the solution of Eq. (130) by perturbation. For this purpose, we introduce a slow time t_2, as follows

$$t_2 = \delta^2 t_1 = \delta^3 t, \tag{134}$$

and we expand η in terms of δ as follows

$$\eta = \eta_0(\sigma, t_2) + \delta\eta_1(\sigma, t_2) + O(\delta^2), \tag{135}$$

where η_0 is the solution given by Eq. (132).

Introducing ν_0 as follows

$$\nu = \nu_0 \delta^2, \tag{136}$$

and inserting Eq. (135) in Eq. (130), we obtain

at order 0 of δ:

$$\frac{\partial \eta_0}{\partial t_1} + \frac{3}{4}\nu_0\eta_0\frac{\partial \eta_0}{\partial \sigma} + \frac{1}{6}\frac{\partial^3 \eta_0}{\partial \sigma^3} = 0, \tag{137a}$$

and, *at order 1 of δ:*

$$\frac{\partial \eta_1}{\partial t_1} + \frac{3}{2}\nu_0\eta_0\frac{\partial \eta_1}{\partial \sigma} + \frac{3}{2}\nu_0\eta_{0,\sigma}\eta_1 + \frac{1}{4}\nu_0\frac{\partial^3 \eta_1}{\partial \sigma^3} = -\eta_{0,t_2} - \frac{s_0}{2}\epsilon\Delta_0^2\eta_{0,\sigma\sigma}. \tag{137b}$$

Introducing operators $\widehat{L}_0$ and $\widehat{L}_1$ as follows

$$\widehat{L}_0 = \frac{\partial}{\partial t_1} + \frac{3}{4}\nu_0\eta_0\frac{\partial}{\partial \sigma} + \frac{1}{6}\frac{\partial^3}{\partial \sigma^3}, \tag{138a}$$

$$\widehat{L}_1 = \frac{\partial}{\partial t_1} + \frac{3}{2}\nu_0\left(\eta_0\frac{\partial}{\partial \sigma} + \eta_{0,\sigma}\right) + \frac{1}{4}\nu_0\frac{\partial^3}{\partial \sigma^3}. \tag{138b}$$

Eqs (138a) and (138b) read

$$\widehat{L}_0 \eta_0 = 0, \tag{139a}$$

$$\widehat{L}_1 \eta_1 = -\eta_{0,t_2} - \frac{s_0}{2} \epsilon \Delta_0^2 \eta_{0,\sigma\sigma}. \tag{139b}$$

To go further, we apply Green's theorem in one dimension. One can find the application of this theorem to linear differential operators in various works [44–46]. In particular, the damping of solitary waves [48, 49] has been shown using this theorem and an extension to matrix differential operators has been performed by [8].

Applying Green's theorem to our case by replacing Eqs (138a) and (138b) in Eq. (95), yields

$$\int_{-\infty}^{+\infty} \left(\eta_0 \widehat{L}_1 \eta_1 - \eta_1 \widehat{L}_0 \eta_0 \right) d\sigma = 0. \tag{140}$$

Notice that the right hand side of (140) is null due to the symmetric behaviour of η_0 and η_1 at $\pm\infty$. Replacing η_0 by Eq. (132) with a time dependant amplitude $a(t_2)$, Eq. (140) yields:

$$a(t_2) = \frac{1}{1 - \frac{2}{5} \frac{s\epsilon\Delta^2}{\delta^2} t_2}. \tag{141}$$

Using the approximation $O(\nu) = O(\delta^2)$, Eq. (134) can equivalently be written as $t_2 = \nu\delta t$. Hence, Eq. (141) becomes

$$a(t) = \frac{1}{1 - \frac{t}{t_b}}, \tag{142}$$

where

$$t_b = \frac{5\delta}{2\epsilon s \Delta^2 \nu}. \tag{143}$$

From Eq. (142), it can be seen that the amplitude $a(t) \to \infty$, when $t \to t_b$ which we call the blow-up time. Hence, the solution of (128a) reads:

$$\eta = a(t) \cosh^{-2}(\theta), \tag{144}$$

where

$$\theta(x,t) = \alpha a^{1/2} \left[x - t + \frac{\nu}{2} t_b \ln \left(1 - \frac{t}{t_b} \right) \right], \qquad \alpha = \left(\frac{3}{4} \frac{a_0}{h} \right)^{1/2} \frac{\lambda_0}{h}, \tag{145}$$

5.2 Blow-up in finite time and the evolution of the solitary wave solution's shape

In this section we shall study the evolution of the soliton-like solution's shape in time , Eq. (144), before the blow up time t_b.

Coming back to variables with dimensions, Eq. (117), the solution of KdV-B, i.e. Eq. (144) reads:

$$\eta(x,t) = \frac{a_0}{1 - \frac{t}{t_b}} \cosh^{-2}\left\{ \frac{\alpha}{(1 - \frac{t}{t_b})^{1/2}} \frac{1}{\lambda_0} \left[x - c_0 t + \frac{\nu}{2} c_0 t_b \ln\left(1 - \frac{t}{t_b}\right) \right] \right\}. \tag{146}$$

For $t = 0$, we have

$$\eta(x,0) = a_0 \cosh^{-2}\left(\frac{\alpha}{\lambda_0} x \right), \tag{147}$$

where

$$\alpha^2 = \frac{3\nu}{4\delta^2} = \frac{3}{4} \frac{a_0 \lambda_0{}^2}{h^3}. \tag{148}$$

Using Eq. (148), the blow-up time, t_b can also be expressed as follows for further use:

$$t_b = \frac{5}{2} \frac{c_0 h^2}{\epsilon s a_0 \Delta^2}. \tag{149}$$

The wave number k and the frequency ω, for a monochromatic progressive wave with a phase $\theta(x,t) = kx - \omega t$, are defined as follows:

$$k = \frac{\partial \theta}{\partial x}, \qquad \omega = -\frac{\partial \theta}{\partial t}. \tag{150}$$

These definitions can be generalized for k and ω depending on x and t:

$$k(x,t) = \frac{\partial \theta}{\partial x}(x,t), \qquad \omega(x,t) = -\frac{\partial \theta}{\partial t}(x,t). \tag{151}$$

Using Eqs (151), (145) and (142), the wavelength $\lambda(t)$ and the wave number $k(t)$ of the soliton-like solution (144) are

$$\lambda(t) = \frac{\lambda_0}{\alpha}\left(1 - \frac{t}{t_b}\right) = \left(\frac{4h}{3a_0}\right)^{1/2} h \left(1 - \frac{t}{t_b}\right)^{1/2}, \tag{152}$$

$$k(t) = \left(\frac{3a_0}{4h}\right)^{1/2} \frac{1}{h} \left(1 - \frac{t}{t_b}\right)^{-1/2} = \alpha a^{1/2}(t). \tag{153}$$

We define the effective wave number, noted $\widetilde{k}$, as follows:

$$\widetilde{k} = \frac{\alpha}{\lambda_0} = \left(\frac{3a_0}{4h}\right)^{1/2} \frac{1}{h}, \tag{154}$$

and we define the associated effective wavelength, noted $\widetilde{\lambda}$, defined as follows:

$$\widetilde{\lambda} = \frac{1}{\widetilde{k}} = \left(\frac{4h}{3a_0}\right)^{1/2} h. \tag{155}$$

It worth noticing that for $t \to t_b$, Eqs (152), (153) and (142) give

$$\lim_{t \to t_b} \lambda(t) = 0, \qquad \lim_{t \to t_b} k(t) = \infty, \qquad \lim_{t \to t_b} a(t) = \infty, \tag{156}$$

respectively. This is the first indication of the narrowing of the solitary wave solution's shape while its amplitude $a(t)$ grows.

To go further, we are going to examine the speed of phase planes on either side of the soliton-like solution's crest. Using Eq. (153), it is useful to write Eq. (145) as a function of $k(t)$ as follows

$$\theta(x,t) = k(t)(x-t) + \nu t_b k(t) \left[\ln(x) - \ln(k(t))\right]. \tag{157}$$

Using Eq. (153), we have

$$\frac{\partial k(t)}{\partial t} = \frac{k^3(t)}{2\alpha^2 t_b}. \tag{158}$$

Eqs (151) and (158) together, yields ω as a function of $k(t)$:

$$\omega(x,t) = -\frac{k^3(t)}{2\alpha^2 t_b}(x-t) + k(t) - \nu t_b \frac{k^3(t)}{2\alpha^2 t_b}\left[\ln\left(\frac{\alpha}{k(t)} - 1\right)\right]. \tag{159}$$

The dimensionless phase velocity $c(x,t)$ of the soliton-like solution is

$$c(x,t) = \frac{\omega(x,t)}{k(t)} = 1 + \frac{\nu}{2\alpha^2}k^2(t) - \frac{k(t)\theta(x,t)}{2\alpha^2 t_b}, \tag{160}$$

which, by using Eq. (153), can equivalently be written as a function of $a(t)$ as follows

$$c(x,t) = 1 + \frac{\nu}{2}a(t) - \frac{a^{1/2}(t)}{2\alpha t_b}\theta(x,t). \tag{161}$$

The position of solitary wave's crest is found by solving

$$\theta(x,t) = 0, \tag{162}$$

at any time t. The dimensionless phase θ is given by the first of the equations in Eq. (145), while the phase velocity c is given by Eq. (161). Therefore, the position of the solitary wave's crest and the velocity of the solitary wave at it's crest are

$$x_{crest}(t) = t + \frac{\nu t_b}{2}\ln[a(t)], \tag{163}$$

$$c(x_{crest}, t) = 1 + \frac{\nu}{2}a(t), \tag{164}$$

respectively.

Using Eqs (161) and (145), the phase speed becomes:

$$
\begin{aligned}
c &= c_{crest} - \frac{\alpha}{2}\frac{a(t)}{t_b}\left[(x-t) - \frac{\nu}{2}t_b \ln\left[a(t)\right]\right] \\
&= c_{crest} - \frac{\alpha}{2}\frac{a(t)}{t_b}\left[x - x_{crest}\right].
\end{aligned}
\tag{165}
$$

Therefore, the speed of the phase planes at $(x_{crest} - \Delta x)$ and $(x_{crest} + \Delta x)$ are

$$
c_{crest-\Delta x} = c_{crest} + \frac{\alpha}{2}\frac{a(t)}{t_b}\Delta x,
\tag{166a}
$$

$$
c_{crest+\Delta x} = c_{crest} - \frac{\alpha}{2}\frac{a(t)}{t_b}\Delta x,
\tag{166b}
$$

respectively. Hence,

$$
c_{crest-\Delta x} > c_{crest} > c_{crest+\Delta x}.
\tag{167}
$$

This means that the phase planes at the left side of x_{crest} have greater speed than the phase planes at the right side of x_{crest} resulting to a narrowing the soliton-like solution's shape while it's amplitude $a(t)$ grows (Figure 7).

At the first glance, the wave breaking does not result directly from the solitary wave solution of KdV-B equation. However, knowing that we have an *accelerating* solitary wave at the speed c_{crest}, the breaking might result from phase planes with non equal accelerations. This will be the subject of fore coming studies.

In the following subsections, various criteria of wave breaking are reviewed.
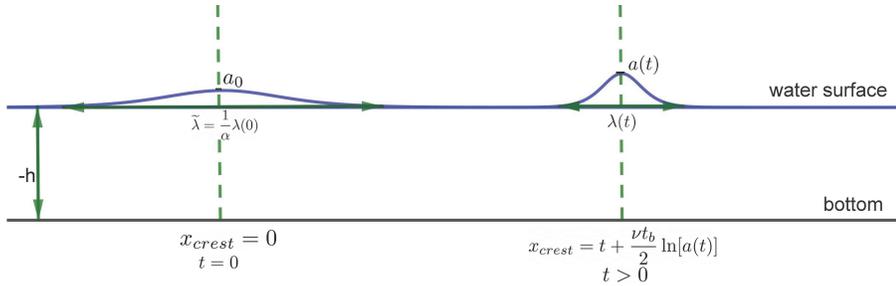

Figure 7. On the left, the soliton-like solution is plotted at $t = 0$. The amplitude at crest is a_0 and its effective wavelength is $\widetilde{\lambda}$. The origin of coordinates is placed at its crest position. On the left side, at $t > 0$, the solitary wave has moved to the right, its shape has sharpened, $\lambda(t) < \widetilde{\lambda}$, and its amplitude has grown, $a(t) > a_0$. Notice that for convenience, scales are not respected.

5.3   Wave breaking criteria

As noticed in the previous section, the wave breaking does not result from the evolution of the wave as the soliton-like solution of KdV-B equation. Therefore, we have to consider

other reasons for the wave breaking. The most well-known criteria of wave breaking for linear monochromatic waves are the McCowan criterium [61], The Miche criterium [62] and the horizontal velocity criterium [63]. But, as we shall see, this latest cannot be applied to our case. Therefore, we propose an alternative criterium that we shall call "alternative velocity criterium". For further use, we call $t_{d,Mc}$, $t_{d,Mi}$ and $t_{d,alv}$, the wave breaking times within McCowan criterium, Miche criterium and alternative velocity criterium, respectively.

In what follows, we shall compute the breaking time t_d, as well as the amplitude, the wavelength and the phase velocity of the solitary wave at $t = t_d$ within each of the mentioned criteria.

5.4   McCowan criterium

The McCowan criterium is established for linear solitary waves and studies the highest maximum height that such waves might attain without breaking. McCowan has shown that the breaking occurs at a given rate between the maximum wave amplitude a_{max} and the water depth h. Namely:

$$\frac{a_{max}}{h} \approx 0.78. \tag{168}$$

Applying this criterium to the soliton-like solution Eq. (146), where $a(t) = a_0(1 - \frac{t}{t_b})^{-1}$, Eq. (168) yields

$$\left(\frac{a_0}{h}\right) \frac{1}{1 - \frac{t_{d,Mc}}{t_b}} \approx 0.78. \tag{169}$$

Eq. (169) gives the breaking time according to McCowan criterium, which is

$$t_{d,Mc} \approx t_b(1 - 1.28\nu). \tag{170}$$

Using Eq. (146), it is easy to calculate the maximum height reached at $t = t_{d,Mc}$. This is

$$\eta_{max} = a_{max} \approx \frac{a_0}{1.28\nu} \approx 0.78h. \tag{171}$$

In addition Eq. (152), one obtains the solitary wave's wavelength at the moment of wave breaking, namely $\lambda(t_{d,Mc})$:

$$\lambda(t_{d,Mc}) \approx 1.28 \left(\frac{4}{3}a_0 h\right)^{1/2}. \tag{172}$$

5.5   Miche Criterium

The Miche criterium is based on empirical observations of linear waves' dispersion relations in a finite depth h with a wave length λ. The Miche criterium fixes the maximum height a_{max} reached by the wave before the break down as follows

$$\left(\frac{a}{\lambda}\right)_{max} = \frac{1}{7} \tanh\left(\frac{2\pi h}{\lambda}\right). \tag{173}$$

In our case, replacing a by $a(t) = a_0(1 - \frac{t}{t_b})^{-1}$, and λ by Eq. (152), in the right side of Eq. (173), we have

$$\left(\frac{a}{\lambda}\right)_{max} = \frac{\nu}{2}(3\nu)^{1/2}\left(1 - \frac{t_{d,Mi}}{t_b}\right)^{3/2}.\tag{174}$$

Now, replacing λ by Eq. (152) in the left side of Eq. (173), using $\nu = a_0/h$, taking $t = t_{d,Mi}$ and expanding the hyperbolic tangent up of $\left(\frac{a}{\lambda}\right)_{max}$ up to order $(3\nu)^{3/2}$, we obtain

$$\frac{1}{7}\tanh\left(\frac{2\pi h}{\lambda}\right) = \frac{1}{7}\frac{\pi(3\nu)^{1/2}}{(1 - \frac{t_{d,Mi}}{t_b})^{1/2}} - \frac{1}{21}\frac{\pi^3(3\nu)^{3/2}}{(1 - \frac{t_{d,Mi}}{t_b})^{3/2}} + O(\nu^{5/2}).\tag{175}$$

Using Eqs (173), (174) and (175), and neglecting terms of higher order than ν, we obtain

$$t_{d,Mi} = t_b\left(1 - \frac{7\nu}{2\pi} - \pi^2\nu\right).\tag{176}$$

The maximum height reached by the wave at $t = t_{d,Mi}$ is

$$\eta_{max} = a_{max} \approx \frac{0.09a_0}{\nu} \approx 0.09h.\tag{177}$$

Using Eqs (174) and (176), the solitary wave's wavelength can be calculated at $t = t_{d,Mi}$, which is

$$\lambda_{max} \approx 4.7 \times 10^{-3}\left(\frac{h}{a_0}\right)^{5/2}h.\tag{178}$$

5.6 Alternative horizontal velocity criterium

The horizontal velocity criterium assumes that the wave breaking occurs when the group velocity of a water plane wave exceeds the speed of the phase plane at crest. In our case, this criterium cannot be applied because, for a solitary wave, at first approach, the group velocity does not mean much. Therefore, alternatively we replace this criterium by an alternative approach which assume that the wave breaking occurs when the fluid horizontal velocity exceeds the phase plane velocity at crest. At this moment, the matter starts to be ejected from the wave.

The phase plane velocity is given by Eq. (161). The phase velocity at crest, i.e. for $\theta(x,t) = 0$, is given be Eq. (164). The horizontal water velocity is given by Eq. (128b). Using Eqs (135) and (119), as well as (134) or equivalently $t_2 = \nu\delta t$, the water velocity can be expanded as follows

$$u_0 = \eta - \frac{\nu}{4}\eta^2 + O(\delta, \delta^2).\tag{179}$$

It can be seen from Eq. (144) that at crest $\eta(\theta = 0) = a(t)$. Hence the alternative velocity criterium reads

$$1 + \frac{\nu}{2}a \geq a - \frac{\nu}{4}a^2\tag{180}$$

the above inequality yields the following quadratic equation

$$a^2 + \left(2 - \frac{4}{\nu}\right)a + \frac{4}{\nu} \geq 0 \tag{181}$$

Taking into account that ν is a small parameter, the solution of Eq. (181) are $a \gtrsim \frac{1}{2}$ and $a \gtrsim \frac{4}{\nu} - \frac{5}{2}$. the first part of the solution is not acceptable since it corresponds to negative times, while the latest, using Eq. (142) and neglecting terms of order ν^2 , gives the breaking time $t_{d,alv}$, as follows

$$t_{d,alv} \approx t_b \left(1 - \frac{\nu}{4}\right). \tag{182}$$

Using Eq. (146), the maximum height reached at $t = t_{d,alv}$ is given by

$$a_{max}(t_{d,alv}) \approx 4h \tag{183}$$

The wave length at $t = t_{d,a}$ is obtained from Eq. (152), and reads

$$\lambda(t = t_{d,alv}) = \left(\frac{1}{3}\right)^{1/2} h. \tag{184}$$

6   Integrability perspectives

Recently, the integrability of a general form of the KdV and NLS equations with forcing involving product of eigenfunctions has been proved [64, 65].

More specifically, in [64] it is proved that the following forced version of NLS is integrable:

$$\mathrm{i}q_t + \frac{\alpha}{2}q_{xx} - \alpha\lambda|q|^2 q = \frac{2\mathrm{i}}{\pi}\int_{\mathbb{R}} \frac{g(t,k)}{a_0(k)}\Phi_1^+(x,t,k)\Psi_1^+(x,t,k)\mathrm{e}^{\mathrm{i}\lambda\left(HG(t,k)|b_0|^2(k)\right)}dk,$$
$$x \in \mathbb{R}, \qquad t > 0, \tag{185}$$

where α is a constant real parameter, $\lambda = \pm 1$, Φ_1^+, Ψ_1^+ are appropriate eigenfunctions,

$$G(t,k) = \int_0^t g(\tau,k)d\tau, \quad b_0(k) = \lim_{x\to-\infty} \mathrm{e}^{2\mathrm{i}kx}\Psi_{10}^+(x,k),$$
$$a_0(k) = \lim_{x\to-\infty} \Psi_{10}^+(x,k), \tag{186}$$

and $(\Psi_{10}^+(x,k), \Psi_{20}^+(x,k))$ are defined in terms of $q_0(x) = q(x,0)$ by

$$\Psi_{10}^+(x,k) = -\int_x^\infty d\xi \mathrm{e}^{2\mathrm{i}k(\xi-x)}q_0(\xi)\Psi_{20}^+(\xi,k),$$
$$\Psi_{20}^+(x,k) = 1 - \int_x^\infty d\xi\lambda\overline{q}_0(\xi)\Psi_{10}^+(\xi,k), \qquad -\infty < x < \infty \quad \mathrm{Im}k \geq 0. \tag{187}$$

Eq. (185) possesses the following Lax pair:

$$X_x + \mathrm{i}k[\sigma_3, X] - QX = 0, \qquad Q = \begin{pmatrix} 0 & q \\ \lambda\overline{q} & 0 \end{pmatrix}, \tag{188}$$

$$X_t + \mathrm{i}\alpha k^2[\sigma_3, X] - \alpha \left(kQ - \frac{\mathrm{i}}{2}(Q_x + Q^2)\sigma_3 \right) X$$
$$= \frac{1}{2\mathrm{i}}(Hg)X\sigma_3 - \frac{1}{2\mathrm{i}}(HgX\sigma_3 X^{-1})X, \qquad x \in \mathbb{R}, \quad t > 0, \quad k \in \mathbb{R}, \tag{189}$$

where Hf denotes the Hilbert transform

$$(Hf)(k) = \frac{1}{\pi} p \int_{\mathbb{R}} \frac{f(l)}{l-k} dl, \qquad k \in \mathbb{R}. \tag{190}$$

And in [65], it is shown that the forced integrable extension of the KdV, namely the following equation is integrable.

$$u_t + \alpha(u_{xxx} + 6uu_x) = d_x(x,t) + 2h_x(x,t), \tag{191}$$

where α is introduced in order to consider the $\alpha = 0$ limit and d and h are defined by

$$d(x,t) = \frac{1}{\pi} \int_{\mathbb{R}} g(t,l)(v_{11}v_{22} + v_{12}v_{21})(x,t,l)dl, \tag{192a}$$

$$h(x,t) = \frac{1}{\pi} \int_{\mathbb{R}} g(t,l)v_{21}v_{22}(x,t,l)dl, \tag{192b}$$

is integrable. The functions v_{ij}, $i,j = 1,2$ are the ij components of the matrix v given by

$$v(x,t,k) = \frac{1}{2} \begin{pmatrix} \phi(x,t,-k) - \frac{1}{\mathrm{i}k}\phi_x(x,t,-k) & \phi(x,t,k) - \frac{1}{\mathrm{i}k}\phi_x(x,t,k) \\ \phi(x,t,-k) + \frac{1}{\mathrm{i}k}\phi_x(x,t,-k) & \phi(x,t,k) + \frac{1}{\mathrm{i}k}\phi_x(x,t,k) \end{pmatrix}, \tag{193}$$

where ϕ is an appropriate solution of the associated Lax pair. Namely, ϕ satisfies

$$\phi_{xx} + (u + k^2)\phi = 0, \tag{194}$$

and

$$\phi_t + \alpha(4\mathrm{i}k^3 - u_x)\phi + \alpha(2u - 4k^2)\phi_x + \frac{1}{2\mathrm{i}}(Hg)\phi - \frac{1}{4\mathrm{i}}[Hg(\phi\widehat{\phi} + \frac{1}{k^2}\phi_x\widehat{\phi}_x)]\frac{\phi_x}{\mathrm{i}k}$$
$$+ \frac{1}{4\mathrm{i}}[Hg(\phi\widehat{\phi} - \frac{1}{k^2}\phi_x\widehat{\phi}_x)]\phi - \frac{1}{4\mathrm{i}}[Hg(\frac{1}{\mathrm{i}k}(\phi\widehat{\phi})_x)]\frac{\phi_x}{\mathrm{i}k} = 0, \tag{195}$$

where the hat denotes evaluation at $-k$.

We have strong indications to think that both the KdV-Burger equation (128a) and the NLS equation (70), with appropriate air and water dynamics and wind/wave interaction can be integrable. This will be the subject of fore coming studies.

7   Conclusions

In the first part of this review paper, our aim was exclusively to derive a linear Miles' theory for waves propagating at finite depth h. Hence, we extended the well-known Miles' theory to the finite depth context under breeze to moderate wind conditions. We have linearized the equations of motion governing the dynamics of the air/water interface problem in finite depth and have studied the linear instability in time of a normal Fourier mode k. The prediction of exponential growth of wave amplitude (or energy) is well confirmed by field and laboratory experiments. As an extension, we have derived an anti-diffusive nonlinear Schrödinger equation in finite depth and found the Akhmediev, Peregrine and Ma solutions for weak wind inputs in finite depth.

In the second part, We derived a SGN fully nonlinear, dispersive and focusing system of equations in the context of the nonlinear dynamics of surface water waves under wind forcing, in finite depth. We found that its soliton-like solution with amplitude, velocity, and effective wavelength increased with time. Antidissipation due to wind action through the sheltering Jeffreys' mechanism increases the amplitude of the solitary wave and leads to blow-up which occurs in finite time for infinitely large asymptotic space. The blow-up time is calculated. As an extension, the anti-diffusive Korteweg-de Vries-Burger equation is derived. we have studied in detail the kinetics of the breaking of the wind/wave solitary wave and reviewed various break-up criteria. Experimentally, it is clear that the breaking will occur before the blow up. The experimental confirmation of the present theory can be tested in existing facilities. We will conduct further investigations in this direction in forecoming studies.

Finally, the perspectives of integrability for the NLS equation and the KdV-B equation have been exposed which also be investigated in forecoming studies.

Appendix: Direct derivation of the anti-diffusive Korteweg-de Vries-Burger equation from Euler Equations

Let us consider *a quasi-linear* air/water system with the air dynamics linearized and the water dynamics considered nonlinear and irrotational. The system is $(2+1)$ dimensional (x, z, t) with x and z the vertical and the horizontal space coordinates. The aerodynamic air pressure $P_a(x, z, t)$ evaluated at the free surface $z = \eta(x, t)$ has a component in phase and a component in quadrature with the water elevation. For an energy flux to occur from the wind to the water waves there must be a phase shift between the fluctuating pressure and the interface. Hence, the energy transfer is only due to the component in quadrature with the water surface, or in other words in phase with the slope. To simplify the problem we consider, following references [3, 30, 66], only the pressure component in phase with the slope on the interface i.e.,

$$P_a = \epsilon \rho_a \Delta^2 \eta_x \quad \text{with} \quad \Delta = [\frac{\kappa U_1}{\sqrt{C_{10}}} - c] \tag{196}$$

where $\epsilon < 1$ is the sheltering coefficient, $c = \sqrt{g/k}\tanh(kh)$, $U_1 = u_*/\kappa$ with u_* the friction velocity, $\kappa \sim 0,41$ the Von Kàrmàn constant, C_{10} the wind-stress coefficient and g the gravitational acceleration. This is nothing more that Jeffrey's sheltering mechanisms.

In order to adimensionalize the equations of motion we introduce dimensionless primed variables: $x = lx', z = hz', t = lt'/c_0, \eta = a\eta', \phi = gla\phi'/c_0, U_1 = c_0 U_1'$ with ϕ the velocity potential and a and l typical wave amplitude and wavelength and $c_0 = \sqrt{gh}$. We define two dimensionless parameters $\nu = a/h < 1$ and $\delta = h/l < 1$. So with this assumption the complete irrotational Euler equations and boundary conditions are (dropping the primes)

$$\delta^2 \phi_{xx} + \phi_{zz} = 0, \quad -1 \le z \le \nu\eta, \tag{197}$$

$$\phi_z = 0, \quad z = -1, \tag{198}$$

$$\eta_t + \nu\phi_x\eta_x - \frac{1}{\delta^2}\phi_z = 0, \quad z = \nu\eta, \tag{199}$$

$$\phi_t + \frac{\nu}{2}\phi_x^2 + \frac{\nu}{2\delta^2}\phi_z^2 + \eta + \delta\epsilon s\Delta^2\eta_x = 0, \quad z = \nu\eta, \tag{200}$$

where $s = \rho_a/\rho_w \sim 10^{-3}$ with ρ_a (ρ_w) the air (water) density. We solve the Laplace equation and its boundary conditions with an expansion in powers of $(z + 1)$, namely

$$\phi = \sum_{m=0}^{m=\infty} (z + 1)^m \delta^m q_m(x, t). \tag{201}$$

Substituting (201) in Eq.(197) and using Eq.(198) we obtain

$$\phi = \sum_{m=0}^{m=\infty} (-1)^m \frac{(z + 1)^{2m}}{(2m)!} \delta^{2m} q_{0,2mx}. \tag{202}$$

Using the kinematic and dynamics boundary conditions Eq.(199) and Eq.(200) and disregarding terms in $\mathcal{O}(\nu\delta^2)$ and $\mathcal{O}(\delta^4)$ we find, with $r = q_{0,x}$, the system

$$\eta_t + \{(1 + \nu\eta)r\}_x - \frac{1}{6}\delta^2 r_{xxx} = 0, \tag{203}$$

$$\eta_x + r_t + \nu r r_x - \frac{1}{2}\delta^2 r_{xxt} + \delta\epsilon s\Delta^2\eta_{xx} = 0. \tag{204}$$

The linear wave solution of (203) and (204) moving to the right is $r(\xi) = \eta(\xi)$, $\xi = x - t$, with η (or r) an arbitrary function of ξ. Now we look for a solution with nonlinear corrections to the orders $\mathcal{O}(\nu)$, $\mathcal{O}(s\delta)$, and $\mathcal{O}(\delta^2)$. Following procedure in reference [52] we obtain

$$r = \eta - \frac{1}{4}\eta^2\nu + \frac{\epsilon}{2}\Delta^2\eta_x s\delta + \frac{1}{3}\eta_{xx}\delta^2 + \mathcal{O}(\nu\delta^2, s^2\delta^2, \delta^4), \tag{205}$$

Substituting (205) in (203) and (204) we obtain a focusing KdV-B equation

$$\eta_t + \eta_x + \frac{3}{2}\nu\eta\eta_x + \frac{1}{6}\delta^2\eta_{xxx} + \frac{s}{2}\delta\epsilon\Delta^2\eta_{xx} = 0. \tag{206}$$

For traveling wave solutions, the action of dissipation or "anti-dissipation" in KdV-B is not of great matter except for the sign of the slope [67]. But the soliton-like solutions under the continuous energy transfer from wind to water, exhibits a blow-up and breaking in finite time.

References

[1] Janssen, P. The Interaction of Ocean Waves and Wind (Cambridge University Press, **2004**)

[2] Jeffreys, H. On the formation of water waves by wind, *Proc. R. Soc.* A107, **1925**

[3] Jeffreys, H. On the formation of water waves by wind (Second paper), *Proc. R. Soc.* A110, **1926**

[4] Phillips, O. On the generation of waves by turbulent wind, *J. Fluid Mech.* 2, **1957**

[5] Miles, J. Generation of surface waves by winds, *Appl. Mech. Rev.* 50, **1997**

[6] Janssen, P. Quasi-linear theory of wind-wave generation applied to wave forecast, *J. Phys. Oceanogr.* 21, **1991**

[7] Belcher, S. & Hunt, J. Turbulent shear flow over slowly moving waves, *J. Fluid Mech.* 251, **1993**

[8] Manna, M. & Latifi, A. Serre-Green-Naghdi Dynamics under the Action of the Jeffreys' Wind-Wave Interaction, *Fluids*, 7, **2022**, https://www.mdpi.com/2311-5521/7/8/266

[9] Latifi, A., Manna, M.A., Montalvo, P. & Ruivo, M. Linear and Weakly Nonlinear Models of Wind Generated Surface Waves in Finite Depth, *J. Appl. Fluid Mech.* 10, **2017**, https://doi.org/10.29252/jafm.73.245.27597

[10] Manna, M.A., Latifi, A. & Kraenkel, R.A. Green–Naghdi dynamics of surface wind waves in finite depth, *Fluid Dyn. Res.* 50, **2018**, https://doi.org/10.1088/1873-7005/aaa739

[11] Manna, M. & Latifi, A. Korteweg–De Vries–Burger Equation with Jeffreys' Wind–Wave Interaction: Blow-Up and Breaking of Soliton-like Solutions in Finite Time, *Fluids*, 8, **2023**, https://www.mdpi.com/2311-5521/8/8/231

[12] Young, I. The growth rate of finite depth wind-generated waves, *Coastal Engineering.* 32, **1997**

[13] Young, I. & Verhagen, L. The growth of fetch limited waves in water of finite depth, Part 2: Spectral evolution, *Coastal Engineering*, 29, **1996**

[14] Ijima, T. & Tang, F. Numerical calculation of wind waves in shallow water, *Coastal Engineering Proceedings, North America*, **2011**, https://journals.tdl.org/ICCE/article/view/2401/2076

[15] Lighthill, J. Waves in Fluids (Cambridge University Press, **1978**)

[16] Charnock, H. Wind stress on a water surface, *Quart. J. Roy. Meteorol. Soc.* 81, **1955**

[17] Fairall, C., Grachev, A., Bedard, A. & Nishiyama, R. Wind, wave, stress, and surface roughness relationships from turbulence measurements made on R/P flip in the scope experiment, *NOAA Technical Memorandum*, ERL ETL-268, **1996**

[18] Garratt, J., Hess, G., Physick, W. & Bougeault, P. The atmospheric boundary layer advances in knowledge and application, *Boundary-layer Meteorology*, 78, **1996**

[19] Tennekes, H. The logarithmic wind profile, *J. Atmos. Sc.* 30, **1972**

[20] Rayleigh, L. On the stability or instability of certain fluid motions, *Proc. Lond. Math. Soc.* XI, **1880**

[21] Thijsse, J. Dimensions of wind-generated waves, *General Assembly Of Association D'Océanographie Physique, Procés-Verbaux*, 4, **1949**

[22] Bretschneider, C. Revised wave forecasting relationships, *Proc. 6th Conference On Coastal Engineering, Gainsville/Palm Beach/Miami Beach, FL.* (ASCE, New York, **1958**)

[23] Young, I. The growth rate of finite depth wind-generated waves, *Coastal Eng.* 32, **1997**

[24] Young, I. Wind generated ocean waves (Elsevier Science & Technology, **1999**)

[25] Donelan, M., Babanin, A., Young, I. & Banner, M. Wave-Follower field measurements of the wind-input spectral function, Part II: Parameterization of the wind input, *Journal Of Physical Oceanography*, 36, **2006**

[26] Pierson, W. & Moskowitz, L. A proposed spectral form for fully developed wind seas based on the similarity theory of S.A. Kitaigorodskii, *Journal Of Geophysical Research*, 69, **1964**

[27] Wu, J. Wind-Stress Coefficients over sea surface from breeze to hurricane, *J. Geophy. Res.* 87, **1982**

[28] Fenton, J. A high-order cnoidal wave theory, *J. Fluid Mech.* 94, **1979**

[29] Francius, M. & Kharif, C. Three-dimensional instabilities of periodic gravity waves in shallow water, *J. Fluid Mech.* 561, **2006**

[30] Miles, J. On the generation of surface waves by shear flows, *J. Fluid Mech.* 3, **1957**

[31] Thomas, R., Kharif, C. & Manna, M.A. nonlinear Schrödinger equation for waves on finite depth with constant vorticity, *Phys. Fluids*, **2012**

[32] Touboul, J., Kharif, C., Pelinovsky, E. & Giovanangeli, J. On the interaction of wind and steep gravity wave groups using Miles' and Jeffreys' mechanisms, *Nonlin. Processes Geophys.* 15, **2008**

[33] Touboul, J., Giovanangeli, J., Kharif, C. & Pelinovsky, E. Freak waves under the action of wind: experiments and simulations, *Eur. J. Mech. B: Fluids*, 25, **2006**

[34] Kharif, C., Giovanangeli, J., Touboul., C., Grade, L. & Pelinovsky, E. Influence of wind on extreme wave events: experimental and numerical approaches, *J. Fluid Mech.* 594, **2008**

[35] Onorato, M. & Proment, D. Approximate rogue wave solutions of the forced and damped Nonlinear Schrödinger Equation fro water waves, *Phy. Lett. A*, 376, **2012**

[36] Akhmediev, N., Eleonskii, V. & Kulagin, N. Exact first-order solution on the nonlinear Schrödinger equation, *Theor. Math. Phys.* 72, **1987**

[37] Peregrine, D. Water waves, nonlinear Schrödinger equation and their solutions *J. Austral. Math. Soc. Ser. B*, 25, **1983**

[38] Ma, Y. The perturbed plane-wave solutions of the cubic Schrödinger equation, *Stud. Appl. Math.* 60, **1979**

[39] Dysthe, K. & Trulsen, K. Note on Breather Type Solutions of the NLS as Models for Freak-Waves, *Physica Scripta*, 82, **1999**

[40] Grinevich, P. & Santini, P. The linear and nonlinear instability of the Akhmediev breather, *Nonlinearity*, 34, **2021**, https://dx.doi.org/10.1088/1361-6544/ac3143

[41] Reul, N., Branger, H. & Giovanangeli, J. Air flow separation over unsteady breaking waves, *Physics Of Fluids*, 11, **1999**, https://doi.org/10.1063/1.870058

[42] Su, C. & Gardner, C. Collisional theory of shock and nonlinear waves in plasma, *J. Math. Phys.* 10, **1969**

[43] Serre, F. Contribution à L'étude des écoulements Permanents et Variables Dans Les Canaux, *La Houille Blanche*, 3, **1953**

[44] Dunkel, O. Some applications of Green's theorem in one dimension, *Bull. Am. Math. Soc.* 8, **1902**, https://doi.org/bams/1183416937

[45] Svendsen, I.A. *Introduction to Nearshore Hydrodynamics* (World Scientific: London, UK, **2005**), https://doi.org/10.1142/5740

[46] Chiang, C.M. *The Applied Dynamics of Ocean Surface Waves* (World Scientific: London, UK, **1992**), https://doi.org/10.1142/0752

[47] Darboux, G. *Leçons sur la Théorie Générale des Surfaces et les Applications Géométriques Du Calcul Infinitésimal* (Legare Street Press, **2023**)

[48] Ott, E.; Sudan, R.N. Nonlinear Theory of Ion Acoustic Waves with Landau Damping, *Phys. Fluids*, 12, **1969**, https://doi.org/10.1063/1.1692358.

[49] Ott, E. & Sudan, R.N. Damping of Solitary Waves, *Phys. Fluids*, 13, **1970**, https://doi.org/10.1063/1.1693097

[50] Green, A. & Naghdi, P.M. A Derivation of Equations for Wave Propagation in Water of Variable Depth, *Fluid. Mech.* 78, **1976**

[51] Branger, H., Manna, M., Luneau, C., Abid, M. & Kharif, C. Growth of surface wind-waves in water of finite depth: A laboratory experiment, *Coast. Eng.* 177, **2022**, https://doi.org/https://doi.org/10.1016/j.coastaleng.2022.104174

[52] Whitham, G. *Linear and Nonlinear Waves* (Wiley: New York, NY, USA, **1974**)

[53] Korteweg, D. & de Vries, G. On the Change of Form of Long Waves Advancing in a Rectangular Canal, and on a New Type of Long Stationary Waves, *Philos. Mag. 39*, **1895**

[54] Benney, D.J. Long waves in liquid films, *J. Math. Phys.* 45, **1996**

[55] Johnson, R. Shallow water waves on a viscous fluid-the undular bore, *Phys. Fluids*, 15, **1972**

[56] Grad, H. & Hu, P. Unified shock in plasma, *Phys. Fluids*, 10, **1967**

[57] Hu, P. Collisional theory of shock and nonlinear waves in plasma, *Phys. Fluids*, 15, **1972**

[58] Wadati, M. Wave propagation in nonlinear lattice, *J. Phys. Soc. Jpn.* 38, **1975**

[59] Karahara, T. Weak nonlinear magneto-acoustic waves in a cold plasma in the presence of effective electron-ion collisions, *J. Phys. Soc. Jpn.* 27, **1970**

[60] Green, A., Laws, N. & Naghdi, P.M. On the theory of water waves, *Proc. R. Soc. A*, 338, **1974**

[61] McCowan, J. On the highest wave of permanent type, *Philos. Mag. Ser. 5*, 38, **1894**

[62] Miche, R. *Mouvement Ondulatoires de la Mer en Profondeur Constante ou Décroissante* (École Nationale des Ponts et Chaussées: Marne-la-Vallée, France, **1944**)

[63] Shemer, L. On kinematics of very steep waves, *Nat. Hazards Earth Syst. Sci.* 13, **2013**

[64] Fokas, A. & Latifi, A. The nonlinear Schrödinger equation with forcing involving products of eigenfunctions, *Open Comm. Nonlinear Math. Phy.* 2, **2022**, https://ocnmp.episciences.org/9884

[65] Fokas, A. & Latifi, A. The Korteweg–De Vries Equation with Forcing Involving Products of Eigenfunctions, *J. Of Math. Phy., Anal., Geom.* 19, **2023**, https://jmag.ilt.kharkiv.ua/index.php/jmag/article/view/998

[66] Kharif, C., Kraenkel, R., Manna, M. & Thomas, R. The modulational instability in deep water under the action of wind and dissipation, *J. Fluid Mech.* 664, **2010**

[67] Jeffrey, A. & Xu, S. Exact solutions of the Korteweg-de Vries-Burgers equation, *Wave Motion*, 11, **1989**